MASTER'S THESIS

Course code: BI309F

Name: Dag Osen Gjetø

A High-Throughput Chemostat Array for Adaptive Laboratory Evolution of Microalgae

---

Date: 16. May 2022

Total number of pages: 80

NORD University

www.nord.no

Abstract

Microalgae are gaining increasing interest for both scientific research and industrial production, but finding the appropriate species for each use can be both time-consuming and challenging. For this reason, improving microalgae strains will be increasingly important over the coming years, and the application of adaptive laboratory evolution for directed acquisition of desired traits can be a valuable tool to this end. Chemostats have proved to be effective tools for adaptive evolution in microorganisms, but are large, complex, and expensive. Here, a compact and low-cost mini-chemostat array developed for strain-characterization of yeast is adapted for cultivating phototrophic microalgae, a novel application, to demonstrate the potential of implementing it for strain improvement. This was done by subjecting *Chlorella vulgaris* under stress conditions in terms of nutrient limitation to mimic research on strain adaption, and the results and lessons learned are discussed to provide a framework for an improved version which could be used for future research.

Keywords:

Adaptive laboratory evolution, nutrient limitation, *Chlorella vulgaris*, chemostats, mini-chemostat array

Index

1 Introduction

1.1 Rationale

Techniques for improving microalgae strains will be of increasing interest to a range of industrial sectors over the coming years, as well as to research. Their appeal comes from their remarkable range of potential, such as sources of biochemicals for the pharmaceutical and nutraceutical industries (Borowitzka, 1995; Mehariya et al., 2021), in the production of biofuels, or to produce pigments and cosmetics (Khan et al., 2018). They have been used as food, both historically and in more recent years (Caporgno & Mathys, 2018; Barkia et al., 2019). From a Norwegian perspective they are garnering interest in aquaculture as components of fish feed, presenting a sustainable alternative to traditional components such as fish meal and -oil, or soy (Sarker et al., 2020; Suzuki, 2018). Additionally, they may also be useful in carbon capture, and are a green and renewable resource which can beneficially contribute to reducing the carbon footprint of all the above-mentioned fields (Sayre, 2010; Lam et al., 2012).

The ability to grow and improve upon domesticated crops has transformed the very core of human nature since the agricultural revolution; its potential now turns to microalgae as we aim to utilize them for industrial applications. The search for appropriate microalgae species for varying uses can be challenging, and requires countless hours of work on sampling, cultivation, and genomic investigation. The application of adaptive laboratory evolution (ALE) to fast-track the directed acquisition of useful traits over a short stretch of time holds great potential for research and development, genomic libraries, and biotechnology (LaPanse et al., 2021).

The key to ALE is to hold as great degree of control over the growth environment as possible, by implementing a selection regime which exposes the culture to the desired selection pressure. If the culture is not tightly controlled, confounding factors may be introduced, making the process more complex and thus exacerbating the analysis of either how the algae have adapted, or what caused them to adapt. It could also cause them to adapt to something else entirely, or fail to grow at all.

Control over the microalgae growth environment is typically achieved by two main modes: batch culturing, or continuous growth (Jeong et al., 2016). Batch culturing results in a slower

growth rate, fluctuating population density and growth conditions, as there is no new input of medium once the culture is growing (Dragosits & Mattanovich, 2013). They will therefore experience a gradual depletion of nutrients, and are typically serially propagated, meaning that, after a period of growth, a small subsample are transferred to new medium which is once again abundant in nutrients; this process could be repeated ad infinitum (Lenski & Burnham 2018).

Batch cultivation is also characterized by being easy to perform, provides an ease of mass cultivation in parallel, is cheap, and requires little equipment (Dragosits & Mattanovich, 2013). Employing deep-well plates would allow growing hundreds of cultures in parallel (Gonzalez and Bell, 2013). Continuous growth, on the other hand, is a more high-maintenance process which requires complex and expensive equipment, more space, accommodates fewer cultures simultaneously, and is more energy-intensive. It does however provide a range of benefits suitable to ALE, such as consistent environmental and nutritional conditions, allowing for constant growth rates (Lee & Kim, 2020). To achieve continuous growth, chemostats and turbidostats are commonly used. These both allow an algae culture to grow continuously, but they differ in one key aspect: while the chemostat is designed to keep the growth conditions constant in terms of nutrient availability by supplying a constant, nutrient-limited stream of medium, the turbidostat is designed to maintain constant turbidity, releasing medium when the culture exceeds a target turbidity value (Skelding et al., 2018).

Continuous growth is the method of cultivation in this project, and to this end, a chemostat system was developed. Using the chemostat for strain adaption is a novel application, and on the whole, use of chemostats in algae research is limited (LaPanse et al., 2021). The chemostat system as a tool for performing ALE was chosen due to its efficiency and consistency, as it allows for continuous growth and a tight control over the selection pressure to which the microorganisms are exposed.

1.2 The chemostat system

The chemostat was first described in 1950 and developed for growing bacterial cultures indefinitely in a liquid suspension (Novick & Szilard; Monod, 1950). After their invention, chemostats eventually fell out of common use, but have seen a resurgence in later years as interest in regulation of cell growth and the molecular basis of adaptive evolution has rejuvenated (Ziv et al., 2013).

Chemostats have historically been, and are today, mostly used for culturing other microorganisms than microalgae. The most commonly used organisms are fungi (specifically yeast, *Saccharomyces cerevisiae*) and various species of bacteria, although the most common is *Escherichia coli* (Dragosits & Mattanovich, 2013). The system is also suited for the cultivation of microalgae, but has historically not been used to the same extent as for cultivating bacteria or fungi (LaPanse et al., 2021). To overcome limitations to the industrial utilization of microalgae, continuous culturing in a chemostat for strain improvement could prove valuable, if the system design can be kept cheap and efficient.

Unlike batch culture growth, where a culture of microorganisms is grown until it reaches a maximum population density before dying (or harvesting), the chemostat is designed for continuous growth over an indefinite period of time. To explain how a chemostat allows continuous growth, a quick summary of its design is necessary (see fig. 1):

The chemostat has a cultivation vessel, which holds a desired volume of suspended microorganisms. Into the cultivation vessel, fresh medium is pumped from a reservoir at a constant rate, replenishing nutrients and compensating for any medium lost through evaporation, splash or human intervention. The chemostat also has a tube for expelling excess culture, commonly referred to as the effluent tube, removing culture at the same rate as medium is pumped in, so the culture does not grow too dense or too dilute.

In addition to this, gas (typically CO_2 and air) is pumped into the vessel to provide aeration and inorganic carbon. Finally, there is a system for mixing the culture, which can take the form of mixing by aeration (bubbling) or mechanical mixing, for instance by using a magnetic stirrer. Mixing the culture is important for even distribution of the algae themselves, as well as the nutrients in the culture. If not mixed, the organisms would slowly sink and settle on the

bottom and walls of the container, reducing growth and creating a gradient imbalance in nutrient content (Rao & Rao, 2004).

The whole system can then be illuminated (either internally or externally) to supply light for photosynthesis, by a light source such as a lamp, or sunlight. Finally, the growth vessel is sealed at the top to stop the medium from evaporating, as well as preventing airborne contamination. With these parameters in place, the chemostat system allows a culture of microalgae to grow at a constant rate under constant, repeatable conditions, for a sustained period of time.

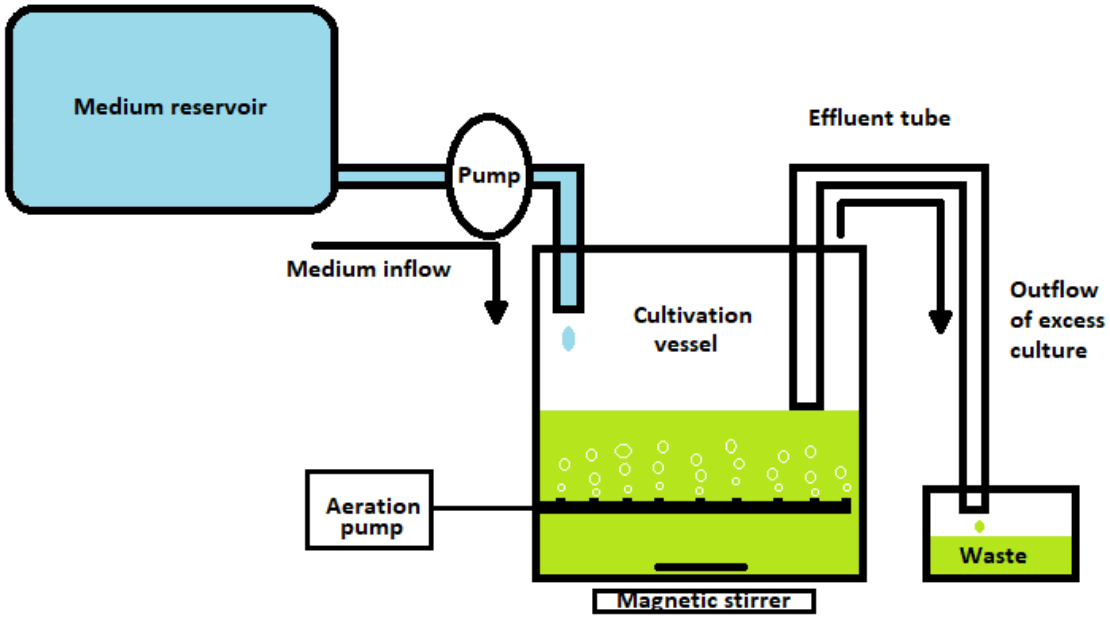

Figure 1 The chemostat and its components; aeration and stirrer are example illustrations, and can differ between chemostat setups

In normal circumstances, i.e. those seen in batch growth, growth of microorganisms follows a model consisting of four phases (fig. 2) (Monod, 1949): The (initial) lag phase, which is a period without noticeable growth where the organism is metabolically active, growing in cell size but not reproducing, adjusting to the new conditions. After the lag phase, the log-phase starts, where the organisms multiply logarithmically until a maximum population density is reached. When this occurs, the growth curve flattens and the culture enters the stationary phase, which is characterized by zero to negative net population growth. After existing for a time in the stationary phase, the death rate will exceed the growth rate, and the population will crash; typically because nutrients are depleted or the culture is too toxic.

In continuous culturing the conditions are as stable as possible, depleted nutrients instantly replenished, fresh medium pumped in, and excess culture being transported out of the growth tube. This results in what is called a "steady-state" of growth, where reproduction virtually never slows down, but remains constant, at a rate equal to the rate of dilution (Novick & Szilard, 1950; Ziv et al., 2013). This state is optimal for studying growth conditions because at constant growth, one can tune the system to change a specific factor to see how growth is impacted.

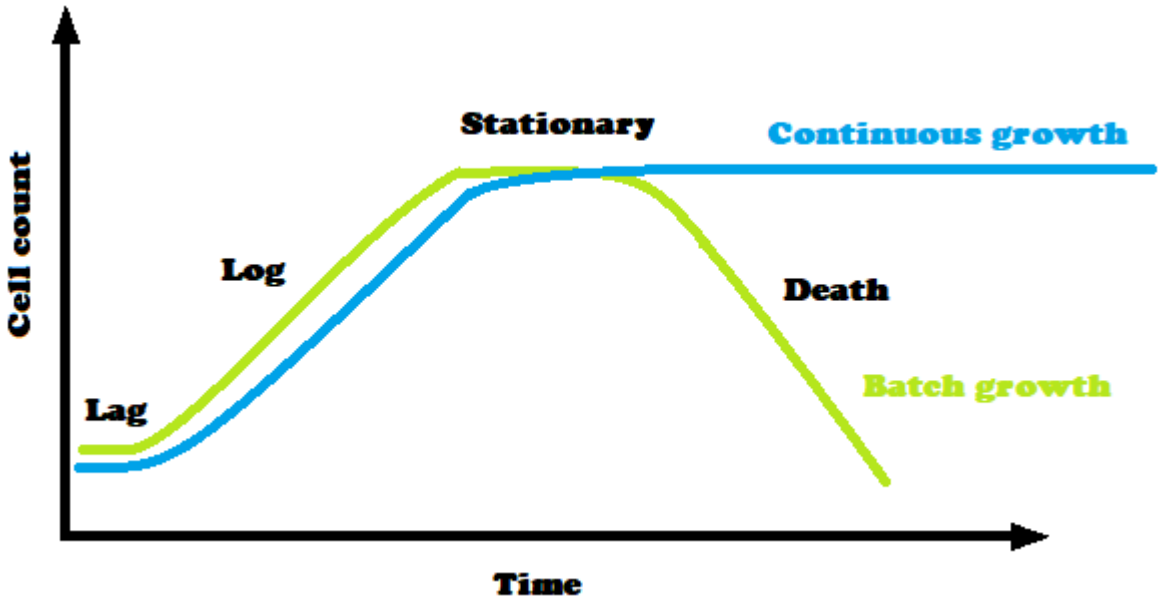

Figure 2 The two growth patterns of microorganisms compared; the green line follows a typical batch growth pattern, whilst the blue line denotes continuous growth.

The four phases (lag, log, stationary, and death) marked along the green line. Note how continuous growth does not enter the death phase, instead entering a "steady-state".
The steady state is the defining state of the chemostat and merits a deeper explanation. As mentioned, at steady state the specific growth rate, μ, is equal to the medium dilution rate (i.e. flow-rate), *D*. *D*, in turn, is the rate at which the volume of the culture is replaced over a specified amount of time, such as per hour or day. Specific growth rate (per day, d^{-1}) occurring at steady state is expressed mathematically by the formula:

$$\mu\,(d^{-1}) = D = \frac{Medium\ flow\ rate\ (L \times d^{-1})}{Culture\ volume\ (L)}$$

To understand why this is, consider microbial growth: the microorganisms will keep multiplying as long as physiological needs are met, i.e. there is sufficient nutrients, and space to grow. As they multiply, their metabolic activity will change their environment, which

eventually limits growth. There are generally three groups of factors limiting growth: Exhaustion of nutrients, accumulation of toxic metabolic products, and changes in pH (Monod, 1949); for phototrophic organisms one must also consider light availability.

In the chemostat, the culture is assumed to be constantly mixed, and have a constant volume due to the inflow/outflow balance. Nutrients are replenished by the inflow, and nutrient availability determines how dense the culture can grow. In other words: nutrient availability is determined by flowrate; thus, flowrate controls culture density.

If the population density is below what the nutrient levels can support, the population keeps growing. If the dilution rate exceeds the growth rate of the microbes, they will be washed out. Hence, the only stable population exists at steady state.

1.3 A novel mini-chemostat array

While chemostats are great tools for investigating microbial growth, they are often large, bulky, complicated or difficult to set up, as well as expensive (Bergenholm et al., 2019). The main aim of the research presented here was to develop a mini-chemostat array used for strain characterization of yeast (Bergenholm et al., 2019), for cultivating phototrophic microalgae. The advantage of the mini-chemostat is chiefly its smaller size and volume, which in a normal chemostat setup ranges between 200 – 1000ml (Bergholm et al., 2019). Each vessel of the mini-chemostat in this project operates with a culture volume of 45 mL, and there are 16 of the vessels operated simultaneously. The principles of the original chemostat are maintained, but are here employed on a much smaller scale, with many replicates growing in parallel. The reduced volume and complexity contributes to reducing costs and allows easier operation.

1.4 Adaptive laboratory evolution (ALE)

The precise control a chemostat gives over the growth environment makes it perfectly suited for directed evolution by allowing the introduction of specific stressors such as an overabundance or lack of certain nutrients, a higher or lower pH than normal, different temperatures, or other environmental factors. The systematic introduction of specific stressors is called *adaptive laboratory evolution* (ALE), and is a powerful tool when used in conjunction with genomics. It utilizes natural selection by forcing the target organism to adapt

to its environment, or die. The ultimate goal is to increase the organism's fitness, under defined conditions, with fitness typically represented by the growth rate. The efficiency of applying ALE is, however, limited by the target organism, which is why microbes are well suited for this purpose. They have simple nutrient requirements, they are easy to cultivate in the lab, and they have typically rapid growth rates, and therefore adapt efficiently to different conditions.

The earliest ALE-experiments are likely the microbial evolution experiments of the Reverend Doctor William Dallinger, published in 1887 (Dallinger, 1887). Rev. Dr. Dallinger wanted to determine whether it would be possible to induce thermal adaptive change in microorganisms, successfully adapting protozoans grown under increasing temperatures for seven years to temperatures far exceeding their ancestral tolerance levels, simultaneously accidentally demonstrating evolutionary trade-offs when noticing that the adapted organisms could no longer grow in the same low temperatures as their ancestors (Bennet & Hughes, 2009). Further improvements to techniques for cultivating microorganisms were made throughout the beginning of the 20th century (Myers & Clark, 1944), and especially relevant for this project, the demonstration of the chemostat in 1950 (Novick & Szilard, 1950a&b). In more recent years, the long-term evolution experiments of professor Lenski are the most famous examples of ALE, providing important insights into evolutionary genetics, adaption, and trade-offs (Lenski et al., 1998; Cooper & Lenski, 2000), exceeding 30 years of cultivation, and 60 000 generations of *Escherichia coli* (Lenski & Burnham 2018).

As with chemostats, the commonest organisms investigated with ALE are bacteria (most notably *E. coli*) and yeast (*Saccharomyces cerevisiae*) (Dragosits & Mattanovich, 2013), with ALE experiments in microalgae being less common, focusing more on acclimation rather than adaption - that is, without genetic change, over a shorter period of time (LaPanse et al., 2021).

The main motivation for inducing genotypic (and consequently, phenotypic) change in algae is to improve production of microalgae-derived products for industry. Processing of microalgae products is optimized, and there is a need for improved techniques to overcome the inherent limitations to their industrial cultivation and utilization (Christi, 2013; Chew et al., 2017; Shurin et al., 2013).

There are several issues facing microalgae cultivation and utilization, which include production parameters, extraction methods, cellular content levels, up- and downregulation of biomass production in combination with optimal extraction methods. There are attempts at combining the production of one class of products, such as biofuels, while utilizing leftovers for producing e.g. pigments, proteins, lipids, vitamins, with value to other industries; but gains are small (Chew et al., 2017). While this is a wide range of issues requiring improvements on multiple fronts, which include issues not related to biology, improving algae strains would certainly address some of the production problems (Radakovitz et al., 2010; LaPanse et al., 2021).

With powerful bioinformatics tools using next-generation sequencing (NGS), allowing us to sequence entire genomes (whole-genome sequencing, WGS), we can read all genetic information contained in an organism (Liu et al., 2012). Theoretically, with total knowledge about an organism's genome and the outcomes of genome manipulation, the target organism could be engineered directly. This has however, yet to be realized; the required changes in genotype in order to create a stable, specific phenotype is complicated, as increasing the yield of a product, or upregulating genes allowing their production, can have severe consequences on growth, which in turn would impact product titers (Mukhopadyay et al., 2008). Likewise, the classic systems-approach to screening a multitude of strains developed through random mutagenesis searching for improved performance, is limited due to the sheer amount of mutants to be screened, as well as the unpredictability of the resulting phenotypes (Kim et al., 2008).

An ALE approach is in comparison a method which yields more stable phenotypes, if not a slower and less (immediately) rewarding process. It also circumvents ethical concerns associated with approaches involving genetic engineering, as genetically modified organisms (GMOs) are subject to restrictions varying from nation to nation, limiting their use and study on the global scale (Zimny et al., 2019).

The greatest advantage of ALE is that genomic change, vis-à-vis phenotypic change, is incredibly complex; therefore an organic approach, where microorganisms are cultivated under well-defined conditions, subject to some kind of selection, better facilitates the emergence of new phenotypes, adapted to the conditions set forth. In this way, phenotypical changes can be associated with the environment and conditions from which they emerged,

and phenotype-genotype correlations can be obtained by genetic screening (Dragosits & Mattanovich, 2013).

Proof of evolution by associating adaption of (phenotypic) traits with a basis in genetic change has been established in this exact way, by screening organisms before allowing them to reproduce and adapt to a limited environment. Interestingly, it was shown that adaptions occur rather quickly at first, then decelerates, while genomic mutation was constant (Barrick et al., 2009). This suggests that ALE might hold an advantage over genetic engineering in terms of strain selection, and is an important method of study to elucidate the complex relationship between genetics and adaption.

1.5 High-throughput data generation and systems biology

Systems biology is a comprehensive quantitative method of analysis, investigating the manner in which the components of a system - the parts of a whole - interact functionally over time. This analysis is carried out in order to understand the emergent properties of a collective, as opposed to the reductionist study of the function of individual parts (Aderem, 2005). A key feature of a systems approach is the generation of massive amount of data for analysis; the chemostat setup allows for the rapid generation of lots of data, and is an excellent tool for continuously generating datapoints about microorganism growth as a function of environmental factors.

The more data we have on a system, the better we can understand its emergent properties. To this end, computational tools and visualization is often necessary to create order out of chaos, as massive datasets on their own will not yield any answers without proper analysis. The analysis can then be repeated on the dataset as it grows, yielding more precise and accurate interpretations for every iteration, helping us understand how changing certain parameters of the system result in phenotypic change, which would be nigh impossible from genome analysis and prediction alone.

Challenges to systems biology include data quality and standardization. Across a field such as microalgal development or strain adaption, this will remain true, but with the mini-chemostat array (if maintained and operated consistently) error can be minimized, and valuable data obtained for selected species.

Applying the chemostat with its rigid parameter controls streamlines data generation as well as theoretically adapting the strains to a certain pressure of choice, such as nutrient- or light limitation. As the chemostat can be made quite small in size, a system containing several chemostat tubes can allow for running multiple experiments with controls in parallel, facilitating high-throughput data generation.

A high-throughput system offers major advantages in research in terms of time and amount of data when compared to serial propagation and batch-growth experiments, and holds great potential in giving rise to new strains adapted to a desired stress. This opens possibilities for genomic analysis and thus uncovering the genetic pathways needed for tolerating the stress under investigation, or could unlock gene clusters related to the production of desired biomolecules.

This means that a high-throughput system for ALE can therefore be a powerful tool for exploring the mutational landscape of a target organism, generating genetic sequences which could be of interest for genomics or even industry via genes induced with biotechnology, or from a business or lab perspective, simply to adapt one's own strains in a time-efficient way.

1.6 Objectives

The overall purpose of this work was to design and test an efficient experimental mini-chemostat (ministat) system for the rapid growth and adaption of microalgae under exposure to stress conditions, intended to provoke phenotypical and genotypic changes towards a desired trait. However, the scope of this project excluded experimental demonstrations of genotypic changes, which would require a lot more time and work. The experimental plan was to demonstrate the basic functionality of the ministat system for phototrophic microalgae, and to investigate how this concept can be further developed, refined, and ultimately utilized as a useful tool in research or industry.

To this end, microalgae were continuously grown under stress conditions, and their ability to cope at different flow rates of medium supply, their response to nutrient stress, and how the algae differ in growth and response under simple treatment differences was then investigated. Parameters include growth rates in terms of biomass and optical density, which will be compared across treatments.

In summary, the project has an outset, and three main goals (fig. 3):
Outset: Build a rudimentary system for microalgal growth, with which the goal is to:

- Operate the system and maintain cultures long term
- Determine if growth can be maintained indefinitely under stress conditions
- Suggest a design for an improved system

And three sub-goals:

- Define and explore growth parameters
- Compare certain endpoints for growth
- Explore whether algae show signs of adaption

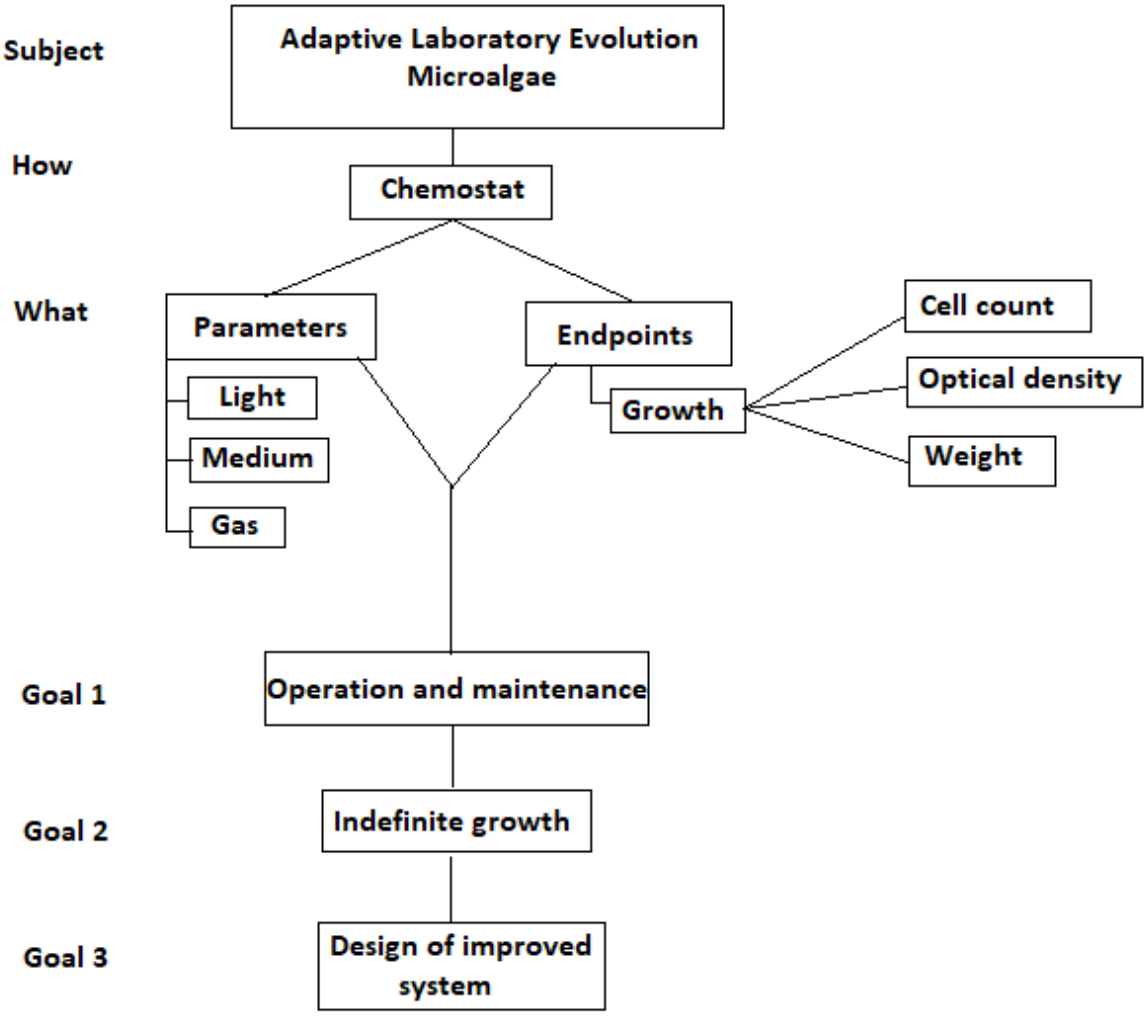

Figure 3 A visualization of project goals and parameters

2 Material and methods

The development of the mini-chemostat array and the experiments occurred in three major phases, which will be referred to throughout this section. Materials and methods has been divided into sections referring to the individual parts of the system, up to the full and operational system.

2.1 Model organism

This initial phase of the project, ("Phase I"), consisted of the acquisition and maintenance of the algae stock. These stocks would supply the first generations of microalgae grown in the chemostat across different runs to ensure consistency in developing baseline growth rates. Phase I also served to establish viability of M8 as a medium for subsequent research.

The organism used was *Chlorella vulgaris* strain CCAP 211/11B (https://www.ccap.ac.uk/). The chlorella were initially cultivated on a shaking table in Erlenmeyer flasks (fig. 4), with three different media (BBM, and M8 with two different nitrogen sources, urea and KNO_3) being tested for suitability as growth medium. Based on the growth of the algae in the flasks (determined by comparing optical density), the decision to use M8 with KNO_3 as nitrogen substrate was taken. Stocks of *C. vulgaris* were then kept in Erlenmeyer flasks growing on M8 KNO_3 (subsequently just "M8") for the duration of the experiments, growing at reduced rates, to be used as inoculants for the mini-chemostat experiments.

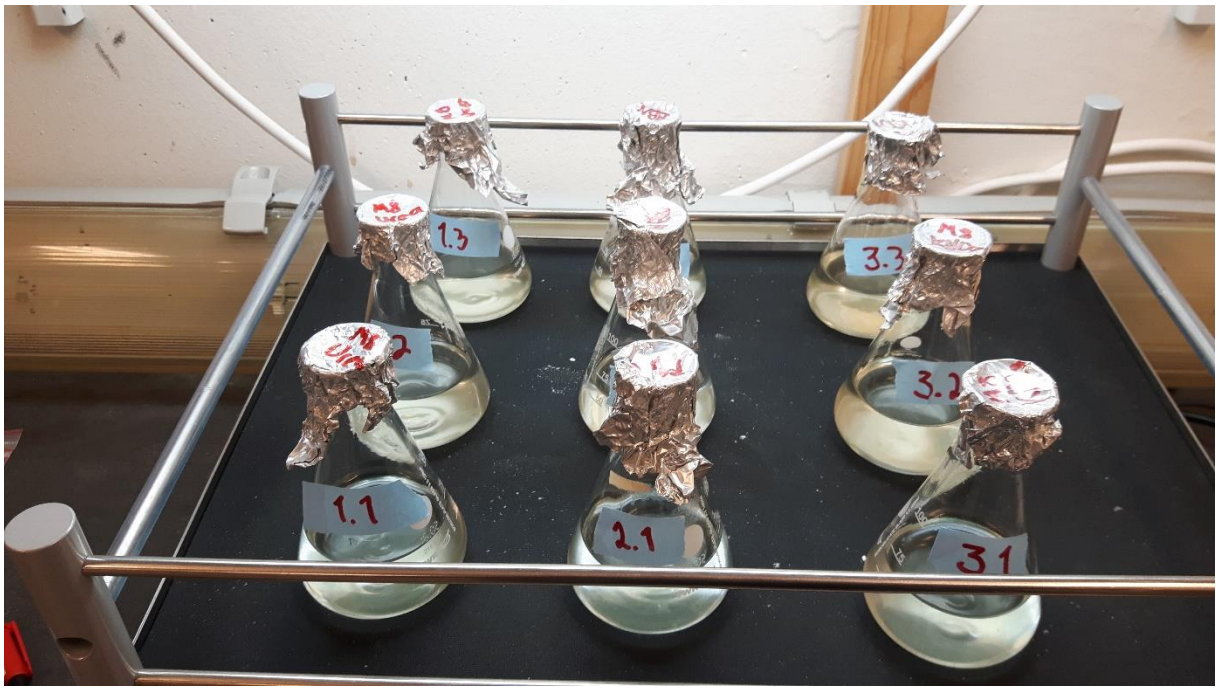

Figure 4 The shaking table with Erlenmeyer flasks containing triplicates of *Chlorella vulgaris* cultures in M8 Urea (1.X), BBM (2.X) and M8 KNO3 (3.X) to be cultivated in the mini-chemostats

2.2 Medium:

The control medium, M8, is based on Mandalam & Palsson (1998) and was made by mixing concentrated stock solutions and deionized water to keep the nutrient content of the growth medium as consistent as possible. The medium was made by measuring up the appropriate amount of deionized water (920 ml per L M8), and mixing in the 4 stock solutions (20ml of each solution per L M8) in order (first stock 1, then stock 2, stock 3, and stock 4), while stirring, and finally adding the nitrogen source, stirring until dissolved. The medium was then autoclaved and left to cool. The recipe (tables 1-5) is described in terms of mg/L, with the stock solutions being a 50x concentration of the original recipe.

Table 1 Stock solution 1 – The Phosphate Buffer solution

Compound	**50x Concentration (mg/L)**	**In finished M8 (mg/L)**
KH_2PO_4	37 000	740
Na_2HPO_4 * $2H_20$	13 000	260

Table 2 Stock solution 2 – Macronutrient solution

Compound	**50x Concentration (mg/L)**	**In finished M8 (mg/L)**
$MgSO_4 * 7H_20$	20 000	400
$CaCl_2$ * $2H_20$	650	13

Table 3 Stock solution 3 – Iron-EDTA solution

Compound	**50x Concentration (mg/L)**	**In finished M8 (mg/L)**
EDTA Ferric sodium salt	5765	115.3
Ne_2 EDTA * $2H_20$	1860	37.2

Table 4 Stock solution 4 – Micronutrients

Compound	**50x Concentration (mg/L)**	**In finished M8 (mg/L)**
H_3BO_3	3.09	0.0618
$MnCl_2$ * $4H_20$	650	13
$ZnSO_4$* $7H_20$	160	3.2
$CuSO_4$ * $5H_20$	90	1.8

Table 5 Nitrogen Source

Compound	**50x Concentration (mg/L)**	**In finished M8 (mg/L)**
KNO_3	NA	3000

In addition to the control medium, reduced media were also created, which were variations of M8 with a reduction of certain nutrients. The reduced media used were named N5, N10, N25, P5, P10, and P25, indicating the component (nitrogen and phosphate, respectively) reduced, as well as the percentage. This was achieved by adding less of stock solution 1 (table 1) in the case of P5, P10, and P25, corresponding to the desired content (5%, 10%, and 25%; i.e. 1ml, 2ml and 5ml /L, respectively) and compensating by adding the same amount of deionized water, and in the case of nitrogen-reduced media, by adding less of the nitrogen-source, KNO_3, where N5, N10, N25 would contain 150mg, 300mg, and 750mg /L, respectively.

2.3 The ministat

Having determined the appropriate growth medium, Phase II was initiated, which involved the construction of the high-throughput ministat system. The first part of this phase was constructing the mini-chemostat (ministat) cultivation vessels, after which the system was tested without a medium supply, but with supplied gas (CO_2 for carbon and air for aeration and mixing).

The individual unit of the mini-chemostat array is the *ministat* (fig. 5). Its components are the cultivation vessel (a 75ml glass tube, with a synthetic sponge cap for sealing) holding the algal culture (45ml); a stainless steel tube with internal diameter (ID) 1.0mm, feeding the gas supply to the bottom of the growth tube to allow for air-lift mixing of the culture. The effluent tube is another stainless steel tube, with an ID of 1.8mm, positioned to the appropriate depth

in the growth tube to remove excess liquid, thus controlling the volume of the culture. Finally, a 20 gauge hypodermic needle (OD 0.908mm) with ID 0.603mm supplies the culture with fresh medium.

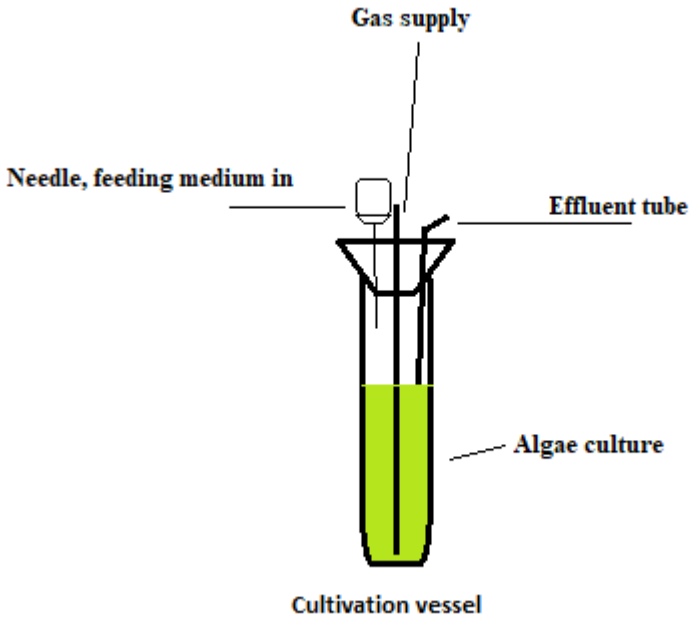

Figure 5 A diagram of the experimental unit, the ministat, consisting of a cultivation vessel, a medium feed, a gas supply tube, and an effluent tube.

2.4 Gas supply

The gas supply was provided by mixing CO_2 from a mass-flow based Gas Mixing System GMS 150 (Photon System Instruments, PSI; fig. 6) with an air supply from an EHEIM air200 aquarium air pump. The CO_2 was provided at a flowrate of 10ml min^{-1} combined with an airflow of 3333.3 ml min^{-1}, mixing the CO_2 with the air (0.3% CO_2 in air). The gas mixture was then pumped through a humidifier, before dividing to the 16 respective ministats through a stainless steel divider with adjustable spigot valves, providing flow control when feeding the gas mixture to growth tubes. Each tube therefore received approximately 209.0 ml min^{-1} air/CO_2 mixture.

Figure 6 The Gas Mixing System GMS 150 (Photon System Instruments, PSI). Can be tuned to output the desired volume of CO_2.

2.5 Pump and medium supply

A Watson Marlow 205 series 16-channel 8-roller pump (fig. 7) was used to feed the medium supply to each ministat. This was achieved by connecting 0.51mm ID pump tubing (Ismatec Pump Tubing, PharMed®) to 1.0 mm ID silicone tubes feeding into the ministat. Each ministat was also fitted with an outflow needle of identical length, and inserted into the tube where it would remove excess liquid above a desired point, so as to keep the volume constant. The culture volume used for all runs was 45mL medium per ministat, and as the volume was so low, the system was vulnerable to volume variation between the replicates, which had to be rigorously controlled; as such, any deviation from normal volume is noted in the results.

Figure 7 The Watson Marlow 205 series 16-channel 8-roller pump

The Watson Marlow medium-pump was initially set to operate at 0.5 rpm, which was found to equal ~7mL of medium /24hrs (0.155 d^{-1}). Outflow was measured to ensure consistency between in- and outflow of medium and culture. The pump speed of medium supply was one of the points of inquiry during the experiments, and ranged from 0.5 to 2.5 rpm; the pump speed is noted in relation to the corresponding growth curves in the results. The dilution rate of the system was calculated by measuring the amount of liquid pumped in over a time period of 1 hour, and repeated for 0.5 rpm, 1.5 rpm, and 2.5 rpm.

2.6 Design of chemostat setup

In Phase III, the full chemostat system became operational, with the addition of a medium supply and the system for in- and outflow of the medium (fig. 8).

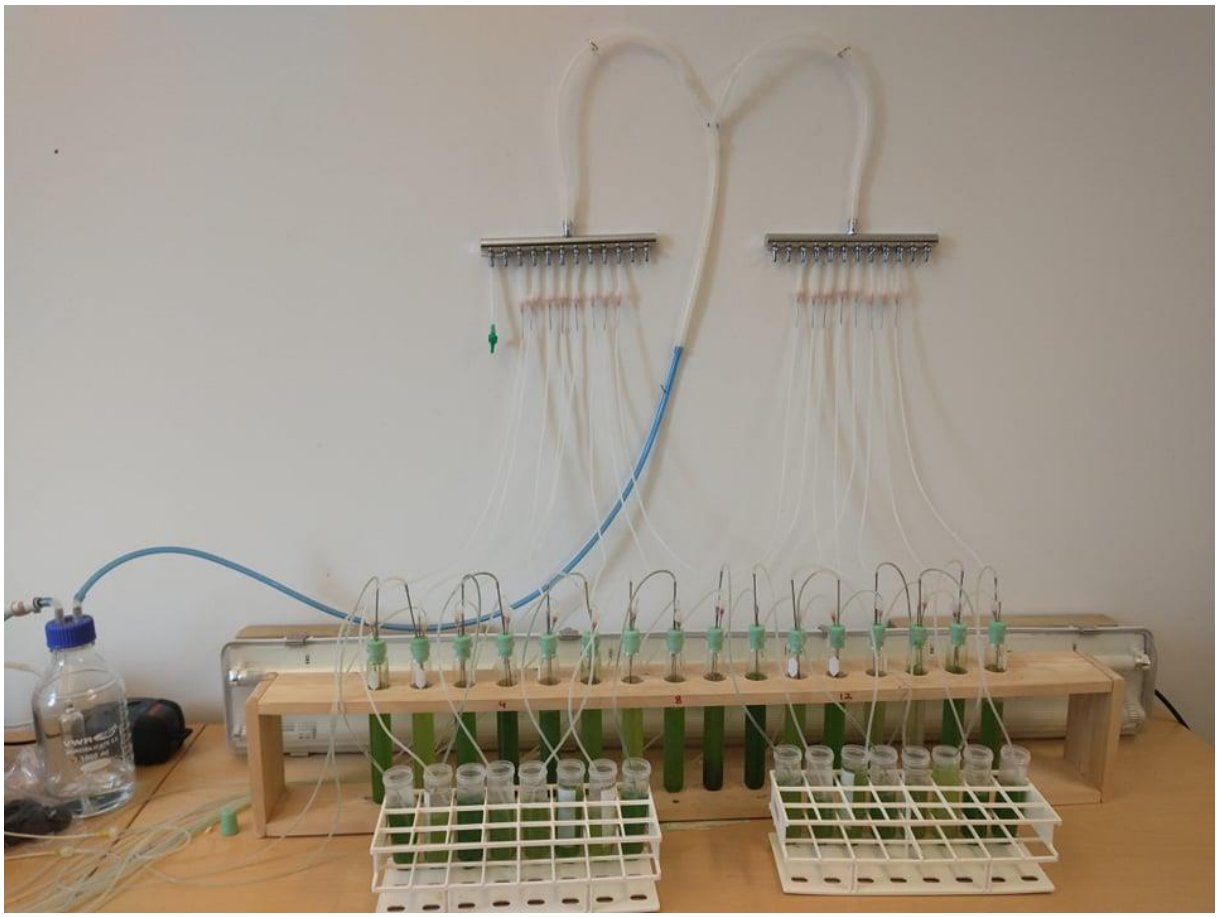

Figure 8 The mini-chemostat array fully assembled.

The system was placed in a room-temperature lab; *Chlorella vulgaris* is a mesophilic species which is easy to work with owing to its remarkable ability to handle harsh conditions and invaders (Safi et al., 2014), making it suitable as a model organism for the purposes of this project.

The mechanical challenge was to get the system flowing properly, and the chemical challenges was to get a stable medium with consistent pH, nutrient availability and to prevent the algae settling, across the different treatments.

The full system is an array of 16 glass tubes, in a rack and placed in front of a lamp to provide light (fig. 9). Distance from the front of tube (facing the lamp) to the lamp was 50mm, and the average light intensity was found to be an average of 140µmol/s/cm^2 (intensity highest in the center of setup (150µmol/s/cm^2), and tapering off towards the ends (135µmol/s/cm^2), in other words fairly uniform. Light was measured with a Li-Cor LI250A light meter and PAR-sensor.

The *C. vulgaris* were for the first four runs grown in the setup with 3 different treatments running in tandem: a control, a nitrogen-reduced treatment, and a phosphorous-reduced treatment (see section, 2.2 Medium). In the fifth and sixth runs, five different treatments were employed, the control and four further nutrient-reduced treatments.

To determine growth, the optical density of the culture was recorded regularly throughout the experiment, as well as dry weight at the initiation and termination of the runs, which each lasted about two weeks in total. The intention was also to record the cell count using Beckman Coulter's Multisizer 3 Coulter Counter (from now referred to simply as "Multisizer"). Unfortunately, due to the Multisizer breaking down, the cell count could not be monitored past the second experiment. The algae were grown until reaching the stationary phase of their growth, at which point the experiment would be terminated and the algae extracted for lipid analysis.

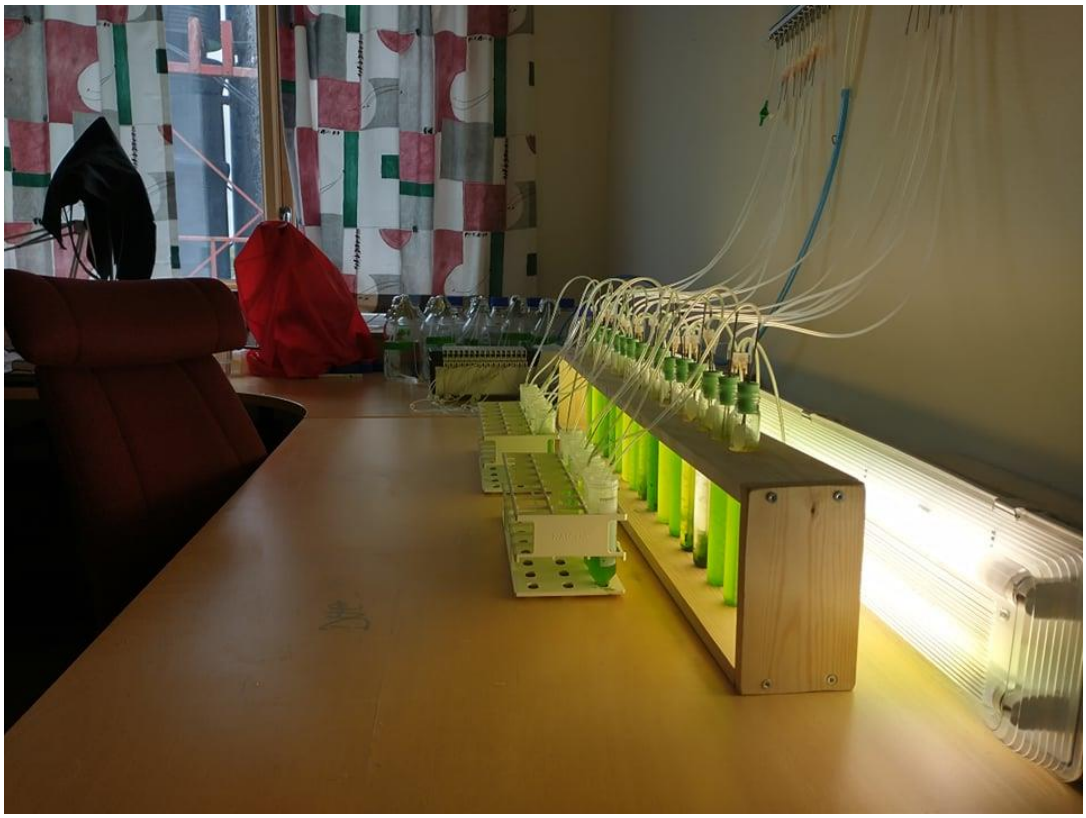

Figure 9 The mini-chemostat array with external lighting and gas supply

2.6.1 Stir tube test run

A test run of a stir-tube was performed as well, to investigate the feasibility of using magnetic stirrers in a small culturing vessel. This was achieved by using a stepper motor and an Arduino UNO USB-board programmed to rotate clockwise at 4 rotations a second for 2 seconds, then counterclockwise for the same amount, before repeating. Magnets were attached to the stepper motor, and a (disinfected) magnet was likewise added to the ministat, placed on top of the stepper motor setup (Fig 10). This ensured magnetic stirring at the bottom of the tube, preventing settling and aiding the bubble mixing.

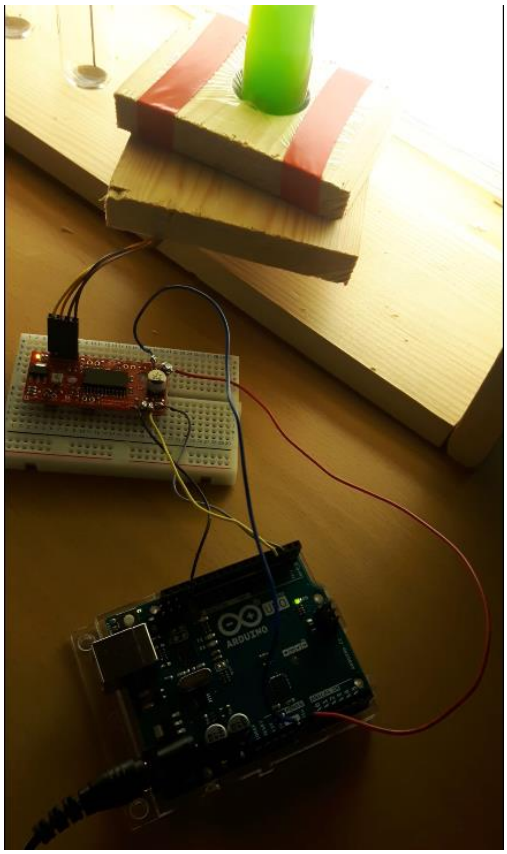

Figure 10 A snapshot of the Arduino UNO-setup with the stepper motor beneath the chemostat, stirring the culture with magnets

2.7 Parameters and analysis:

The parameters measured throughout this project were the following:

- Optical density (all runs)
- Cell counts (only for second run)
- Dry weights (Second, third, fifth, and sixth run)

Based on these parameters, growth curves were plotted. The data was visualized using both Microsoft Excel and R Statistical Software (v. 4.1.2; R Core Team 2021), and statistical analysis performed using R. The R-packages used were “GrowthcurveR” (a custom package for growth curve analysis of batch growth cultures), “stats” (R-standard, contains shapiro.test, Kruskal-Wallis, outlier test, and ANOVA), and “car” (Levene’s test, cook’s distance, and alternate ANOVA-test). Further packages used were “readxl”, “psych”, “ggplot2”, “rgl”, “rockchalk”, “colorRamps”, and “dplyr”.

3 Results

3.1 Batch growth

The first experiment was a batch cultivation which was designed to determine the baseline unconstrained growth rate. The experiment lasted for a total of 337 hours, and the growth data are visualized in figure 11. Data analysis revealed an intrinsic growth rate ranging between 0.015 h^{-1} and 0.016 h^{-1} (0.36 and 0.384 d^{-1}) and a maximum population size ranging from 37 to 67 (measured by light absorption at 540nm wavelength, referred to as optical density, OD) – this is an extremely dense culture (see appendix B, fig. B-1).

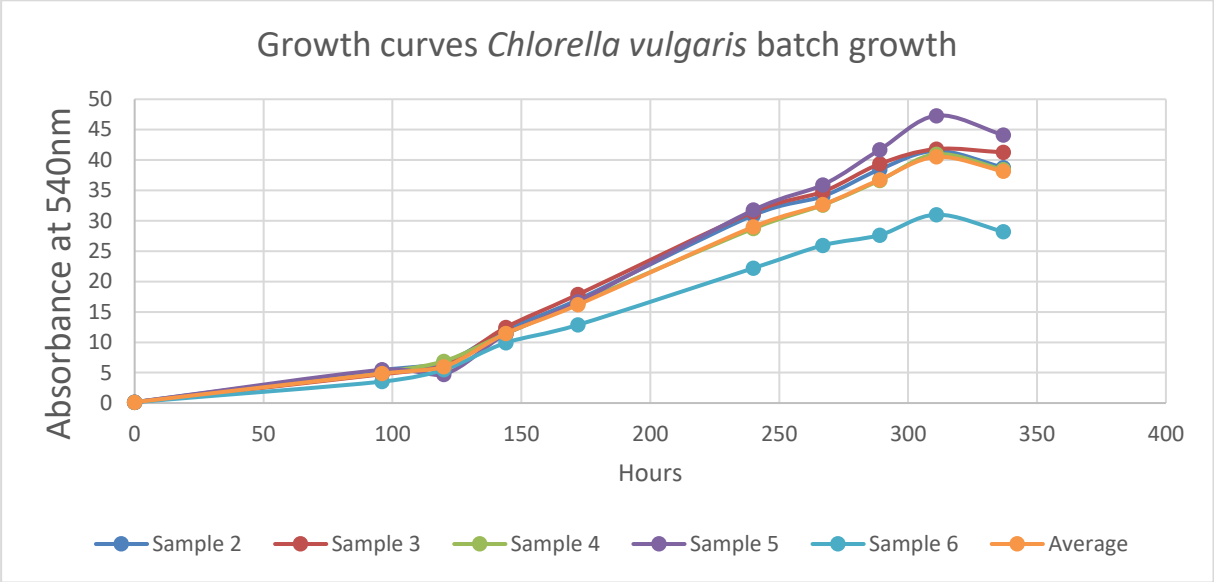

Figure 11 The chart shows the growth of microalgae in terms of optical density (light absorption at 540nm), per hour.

3.2 First continuous ministat test

The first continuous cultivation with chemostat control/constant dilution aimed to demonstrate the functionality of the system for subsequent experiments. The pump speed was set to 0.5 rpm, which was found to be equivalent to 7mL/day, or a flowrate of 0.155 d^{-1}, which is below the maximum growth rate obtained in batch growth (section 3.1). The medium used was normal M8 for all tubes (i.e. only one treatment, the control), with pH measured to 6.21. The duration of the experiment was 359 hours, and the algae stabilized around an OD of 25 (25.475; absorbance at 540nm), and volume stable around 45 mL per tube. The growth curves of the algae are visualized in figure 12.

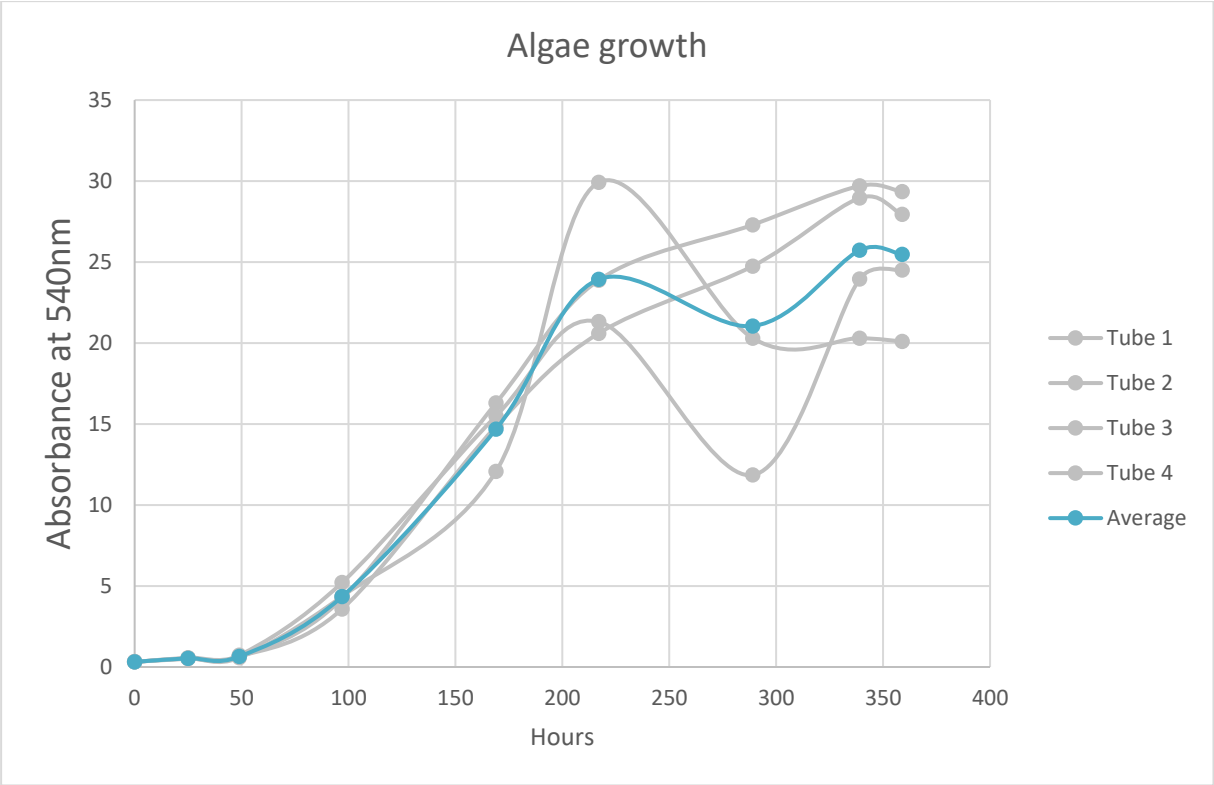

Figure 12 The growth chart of the first continuous run; growth of microalgae in terms of optical density (light absorption at 540nm), per hour. Data in appendix A, table A-1.

3.3 Second continuous ministat test

3.3.1 Light absorption

The second continuous cultivation, which included the implementation of different treatments, with mediums M8 (control), N25, and P25, the latter two of which are variations of M8 developed for this project with reduced nutrient levels. The medium "N25" contained 25% of the nitrogen source (KNO_3) used for M8, and "P25" 25% of the phosphate source (Solution 1 – phosphate buffer solution as outlined in materials and methods, section 2.2). The pH for the media was found to be 6.23 (M8), 6.25 (N25), and 5.96 (P25). The objective of using these reduced nutrient concentrations was to limit the growth rate of the cells and apply stress conditions based on limiting nitrogen and phosphorous resources.

The second continuous cultivation was also the first implementation of all 16 ministats operating simultaneously, and thus a full system test. The pump speed was set to 0.5, equivalent to 7mL/day, or a flowrate of 0.155 d^{-1}. The duration of the experiment was 331 hours, and stationary phase was determined to be reached at approximately 150 hours for both reduced treatments (average absorbance = 19.812 at 540nm), although M8 Control took until approximately 200 hours to catch up.

The cultures showed slight growth after reaching the stationary phase, increasing to average absorbance = 22.603 (at 540nm) at the end of the experiment (331h). Per treatment, the average OD (540nm) at the end of the experiment was 23.64 for M8 (control), 19.10 for nitrogen-reduced M8 (N25), and 24.03 for phosphate-reduced M8 (P25), the growth curves illustrated in figure 13.

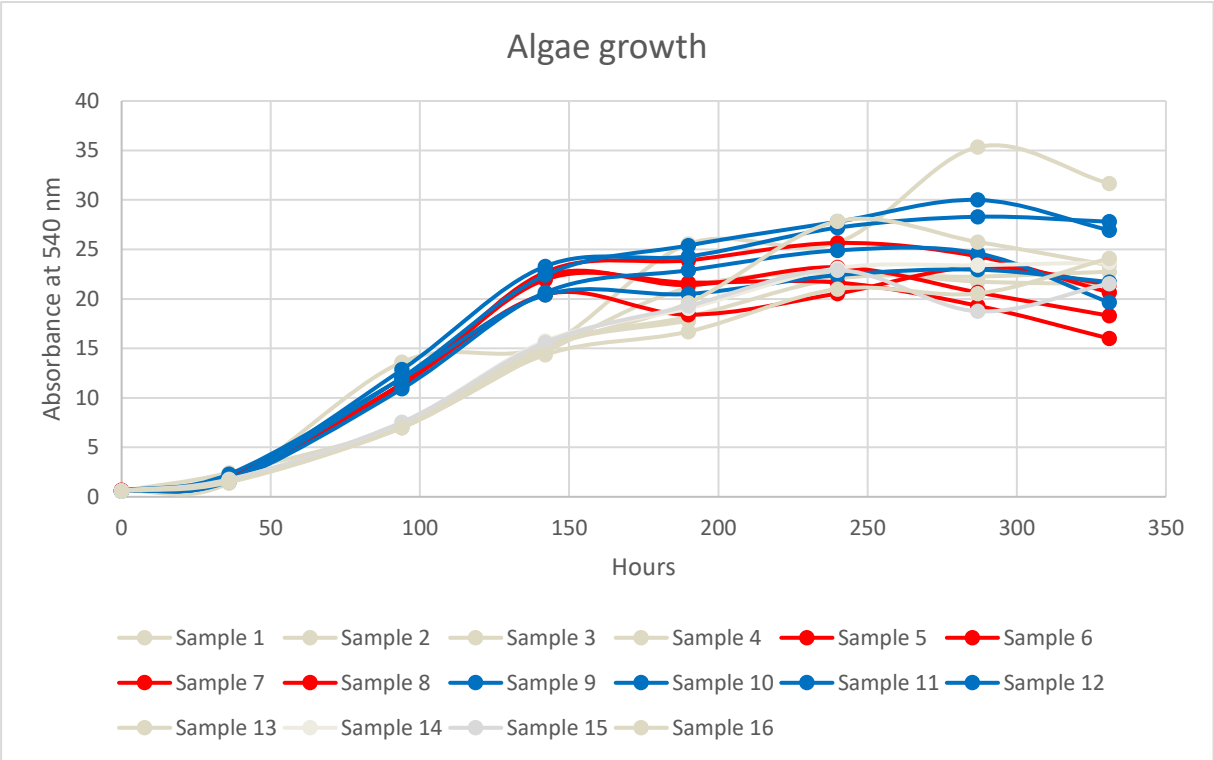

Figure 13 The growth curves of the individual cultures in their ministats, color coded by treatment; Grey samples (1-4, 13-16) represent M8 Control, red samples (5-8) Nitrogen-reduced (25%) cultures, blue samples (9-12) the phosphate-reduced (25%) samples. Data in appendix A, table A-2.

ANOVA of endpoint OD indicate a significant difference in mean values of the control treatment and the N-reduced treatment ($p = 0.0476$), though not with the P-reduced treatment ($p = 0.872$). Dilution rate was 0.155 d^{-1}. Thus, the results indicate nutrient limitation of cell density in N25 treatment, but not in the P25 treatment.

ANOVA-assumptions met with normally distributed residuals ($W = 0.934$; $p = 0.289$; see appendix B fig B-3), and an equal variance ($F = 5.834$; $p = 0.572$; variance ratio < 5 at 2.61, see appendix B, fig. B-3), a boxplot was made to illustrate the difference in OD-range per treatment (fig. 14).

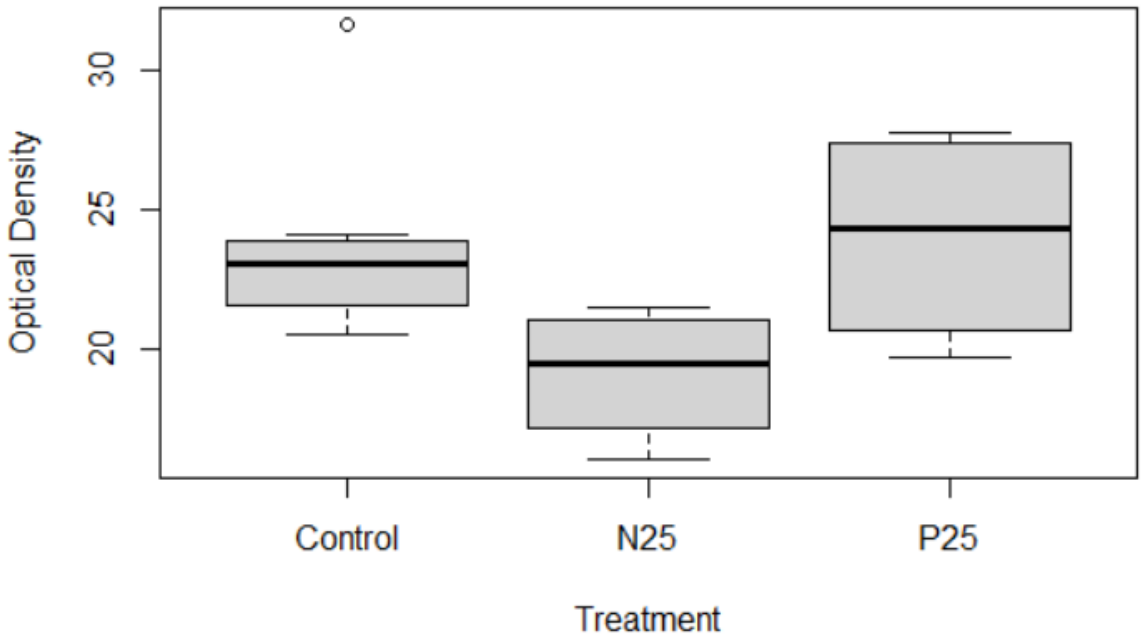

Figure 14 The boxplot compares the means of endpoints (optical density at 331H) by treatment

3.3.2 Dry weights

Samples from the individual cultures were harvested at inoculation (0h) and termination (331h), and the dry weight measured. The dry weight for each sample can be seen in fig. 15, and the net growth (weight at termination minus the weight at inoculation) per treatment in fig. 16. An ANOVA was performed (see appendix B, fig. B-4), returning no significant differences between treatments. Assumptions for ANOVA were met (appendix B, fig. B-5). The dry weights per treatment averaged between 4-5 g/L.

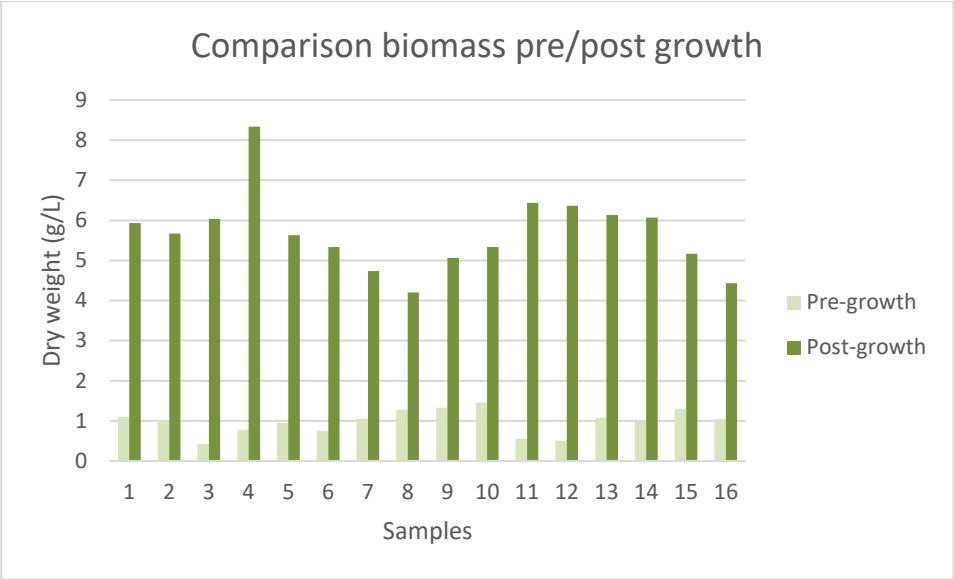

Figure 15 A bar chart showing the total growth of all samples at 0h and 331h. Biomass expressed in g/L. Data in appendix A, tables A-3 and A-4.

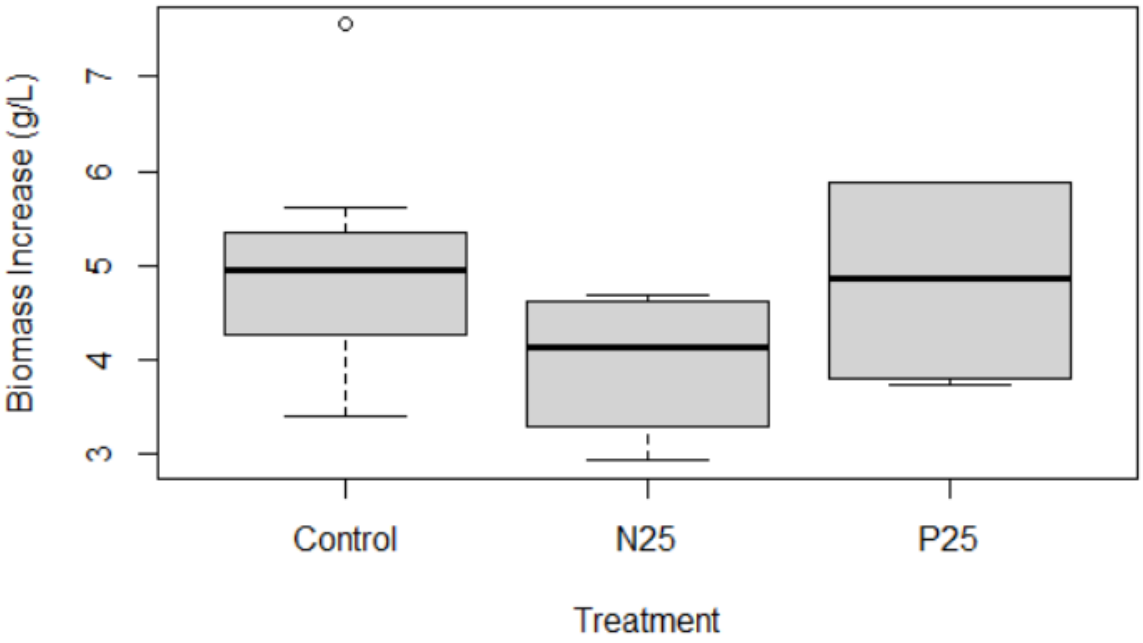

Figure 16 A boxplot comparing the net dry weight increase (in g/L) between the different treatments where C = Control; N = N-reduced (25%); P = P-reduced (25%).

3.4 Third continuous ministat test

3.4.1 Light absorption

The third continuous cultivation also had three different treatments, with media M8 (pH 6.24), N25 (pH 6.30), and P25 (pH 5.94) being utilized. The pump speed was set to 1.5, estimated to be equivalent to 20 mL/day, or a flowrate of 0.44 d^{-1}, which is an increase from previous experiments, and is approximately at the theoretical maximum growth rate as obtained in batch growth (section 3.1). As the medium supply pump is peristaltic, pump efficiency is set by rpm, and an exact match between growth rate and medium supply was hard to achieve. The duration of the experiment was 336 hours, with stationary phase determined to have been reached at approximately 150 hours (average absorbance = 6.968 at 540nm), increasing slightly to average absorbance = 7.163 (at 540nm) at the end of the run (336h), the growth curves illustrated in figure 17. As can be observed, optical densities (absorbance at 540 nm) is lower at 0.44 d^{-1} than at 0.155 d^{-1}.

There were repeated blockage of medium inflow for ministats 13 and 15 (both M8, grey) between hours 72 to 120, reducing inflow of medium and increasing density. The problem was fixed, but the artefact is reflected in the graph (fig. 17), and explains why they made a jump in optical density early on before stabilizing. Samples 4 (M8, grey) and 5 (N25, red) had problems with medium supply leading to low medium turnover and consequently unnatural high density, which spiked out of control as can be observed from the graph (fig. 17).

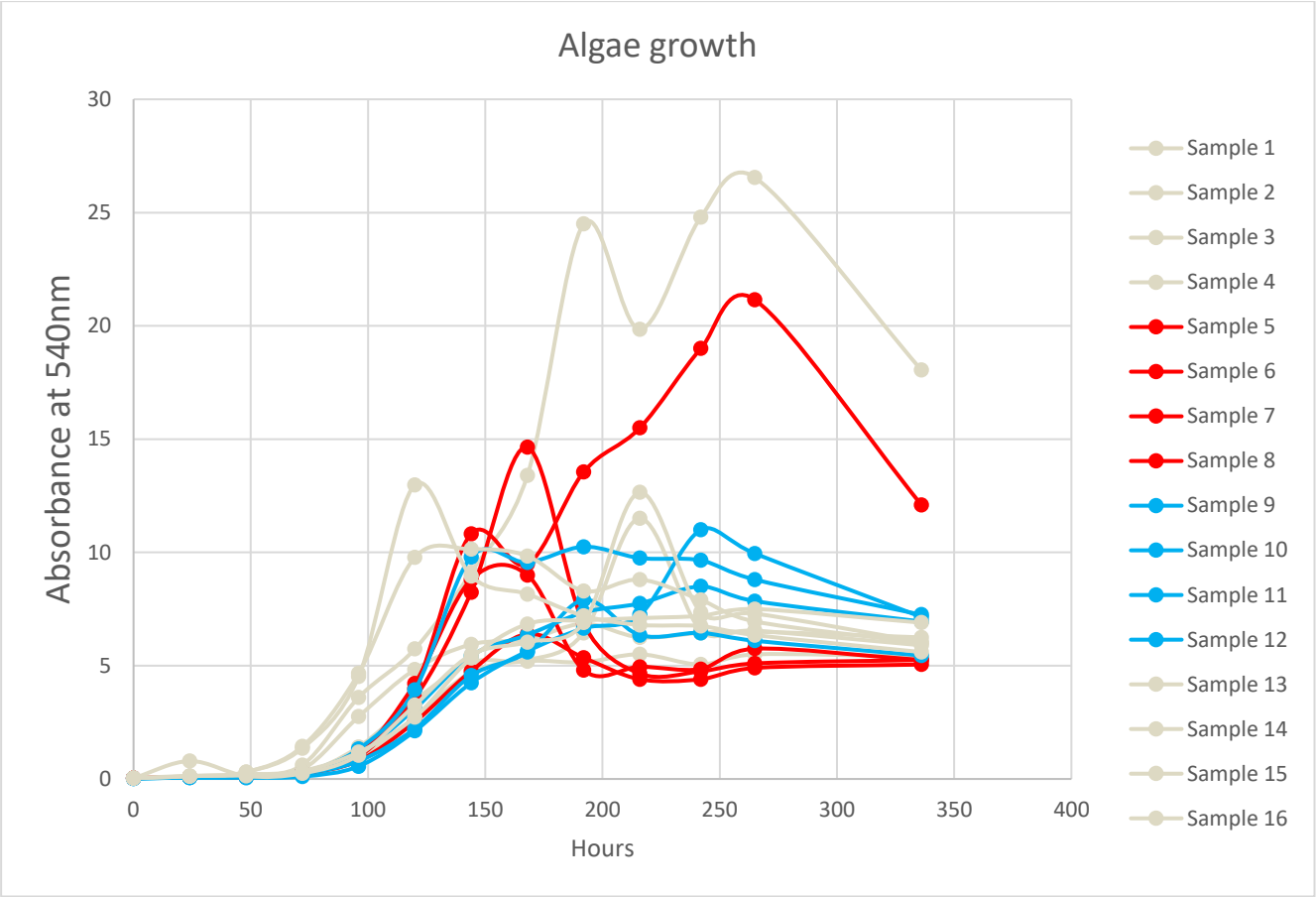

Figure 17 The growth curves of the individual cultures of ministats, color coded by treatment; Grey samples (1-4, 13-16) represent M8 Control, red samples (5-8) nitrogen-reduced (25%) cultures, blue samples (9-12) the phosphate-reduced (25%) cultures. Data in appendix A, table A-7.

ANOVA of endpoint OD (336h), illustrated in the boxplot (fig. 18), indicated no significant difference in mean values between treatments. With the control treatment as intercept, N25 had a p-value = 0.786, and P25 a p-value = 0.714. However, the ANOVA-assumptions were not met, as normally distributed residuals could not be established (p = 2.514e-05); variance was determined to be equal (F-value = 0.205; p = 0.817).

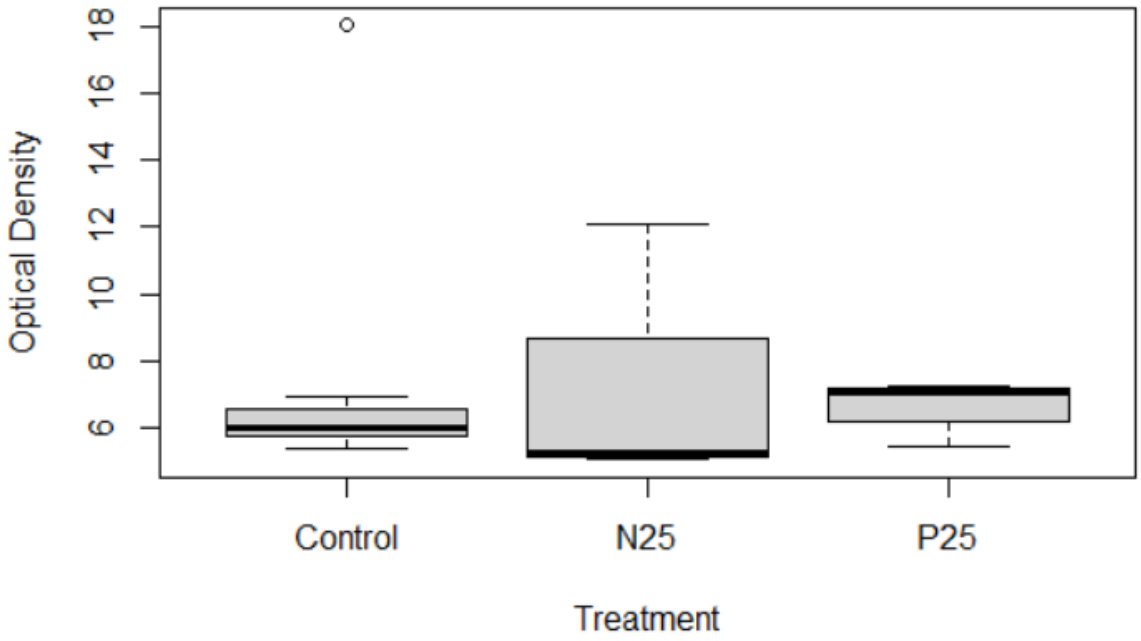

Figure 18 The boxplot compares the means of endpoints (optical density at 336h) by treatment.

As there had been issues with consistent growth due to mechanical errors, and consequently, spikes in culture densities, an outlier test was performed. The test indicated that ministat 4 was an outlier (see appendix B, fig. B-8), which is corroborated by the mechanical problems as mentioned above. The unnaturally high density is apparent in the graph (fig. 17), and is likely a product of reduced medium inflow. The observation was removed, and another outlier test performed, indicating that ministat 5 (designated sample 8 in the R-output in appendix B, fig. B-9 for purposes of grouping) was an outlier also. The observation was then removed as well, and a further outlier test indicated no more outliers (see appendix B, fig. 12).
This new dataset was then graphed (fig 19), and statistics performed on the trimmed data.

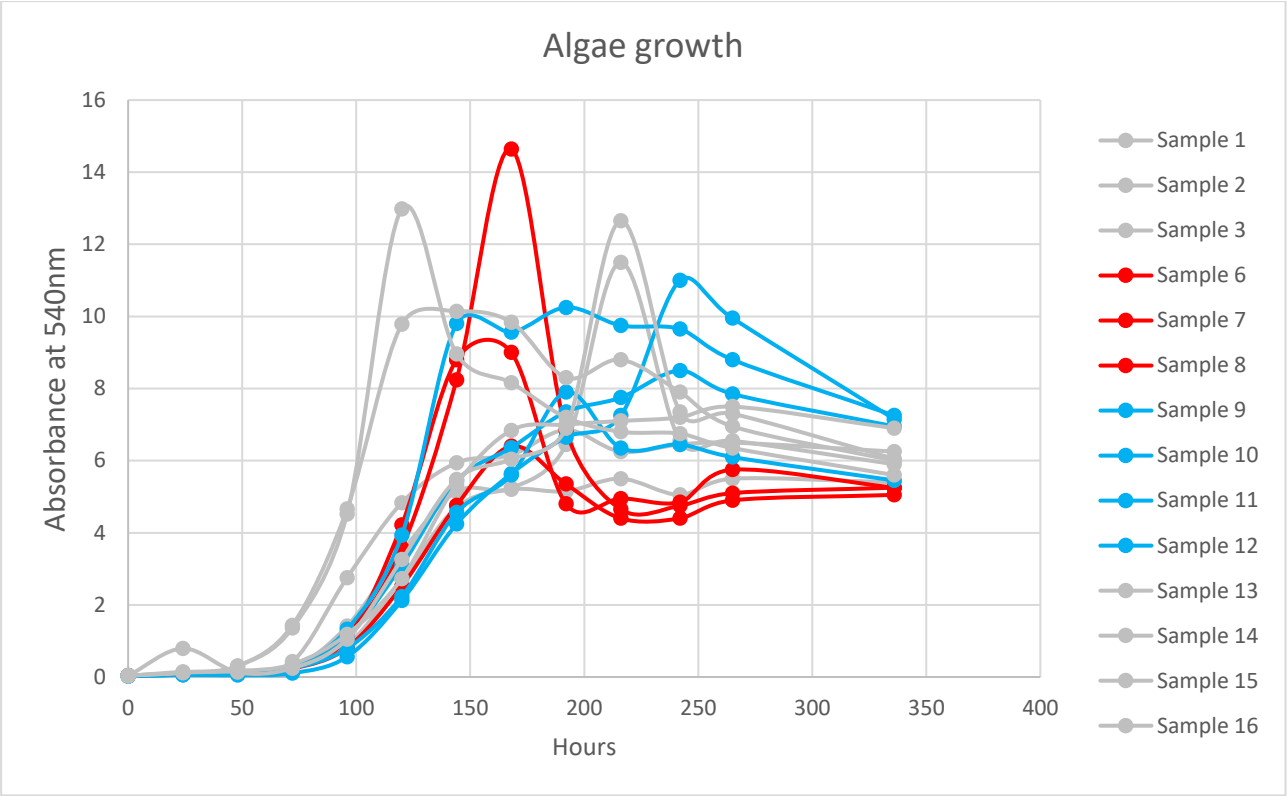

Figure 19 The new growth curves with outliers removed, color coded by treatment; Grey samples (1-3, 13-16) represent M8 Control, red samples (6-8) Nitrogen-reduced (25%) cultures, blue samples (9-12) the phosphate-reduced (25%) samples.

The ANOVA of the new dataset (without the two outliers, samples 4 and 5) indicated that the differences between treatments were too small to be significant (the treatments scoring $p = 0.058$ and 0.081 for N25 and P25, respectively). Both the graph (fig. 19) and boxplot (fig. 20) seem to indicate grouping, but as stated the differences do not fall below the significance threshold of 5% ($p < 0.05$).

Shaprio-Wilks indicated normal distribution of residuals with W=0.95 and p-value = 0.564; and Levene's test indicated equal variance. However, a closer look at the ratio between maximum and minimum variance revealed a ratio of 53.25, which is an extremely high ratio between maximum and minimum variance.

Because the ratio of maximum and minimum variance was so high, a type III ANOVA was performed (see appendix B), which allows for unequal variance. The result indicated that treatment actually was a significant factor in observed optical density, at $p = 0.0165$.
This suggests that when the outliers and unequal variance are accounted for, treatment is significant, after all, and that the observed differences in treatment at this rate of dilution (0.44 d^{-1}) is the product of differences in growth rate as a response to treatment.

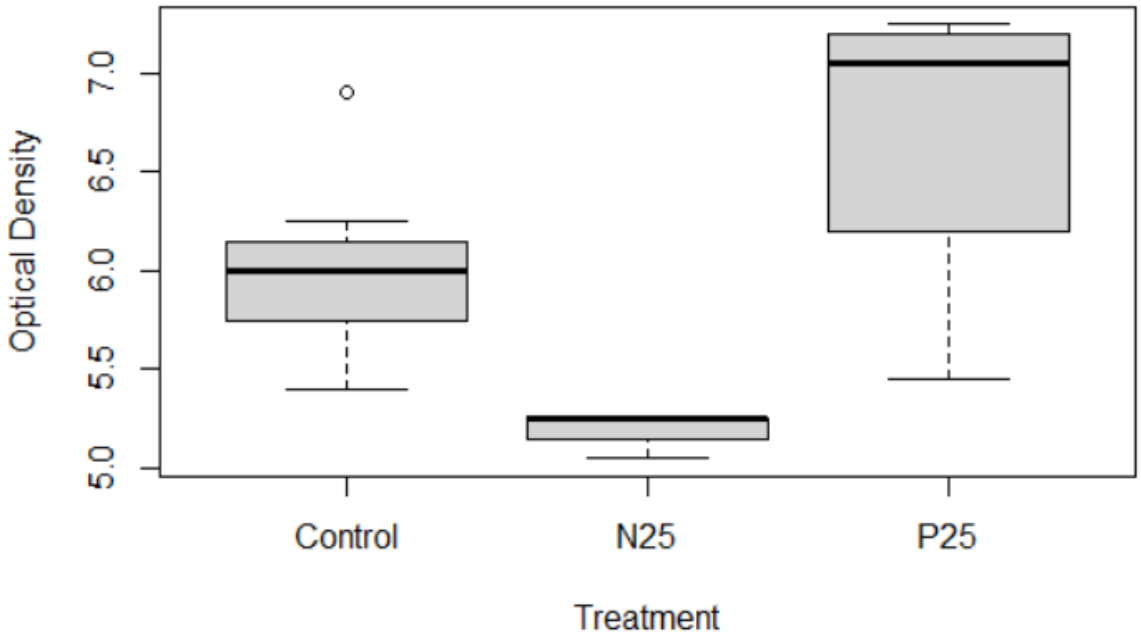

Figure 20 A boxplot of trimmed data (outliers removed), showing growth differences by treatment

3.4.2 Dry weights

Samples from the individual cultures were harvested at inoculation (0h) and termination (336h), and the dry weight measured. The dry weight for each sample can be seen in (fig. 21), and the net growth (weight at termination minus the weight at inoculation) per treatment in (fig. 22). An ANOVA was performed (see appendix B, fig. B-6), returning no significant differences between treatments. Assumptions for ANOVA were met (appendix B, fig. B-7). The dry weights per treatment averaged between 1-2.5g/L.

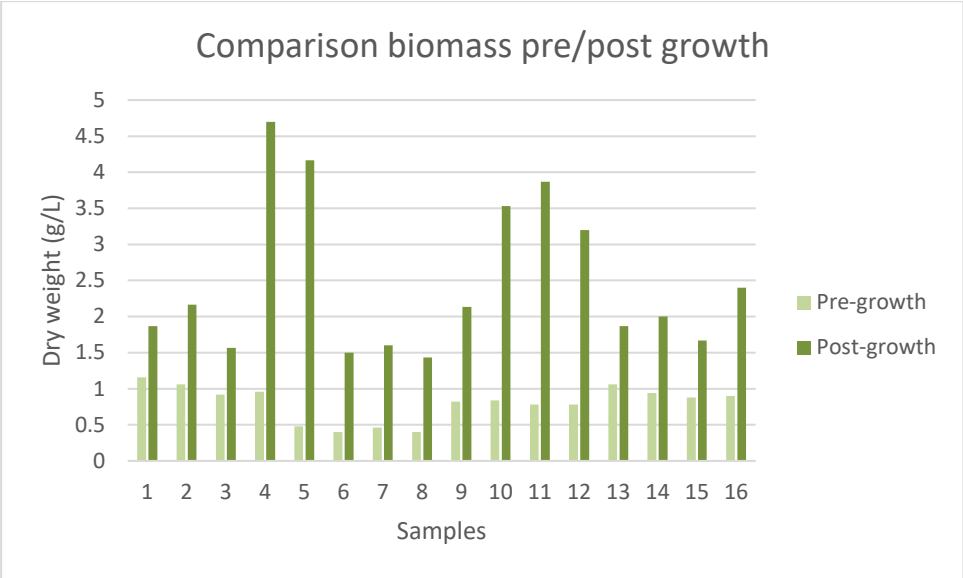

Figure 21 A bar chart showing the total growth of all samples at 0h and 336h. Biomass expressed in g/L. Data in appendix A, tables A-8 and A-9.

Contrasting with the OD-values, samples 4 and 5 were not found to be outliers. This is likely due to the low biomass values, where differences in decimal rounding may lessen or increase differences. However, as outliers were excluded in the OD analysis, they will be excluded for dry weights too for consistency; another analysis of the data with the same samples excluded as for OD-analysis is performed below.

Levene's test indicated homogeneous variance, however, Shapiro-Wilks returned $p = 0.00327$, indicating sample is not normally distributed; this can likely be ascribed to the higher density of the aforementioned outliers (samples 4 & 5).

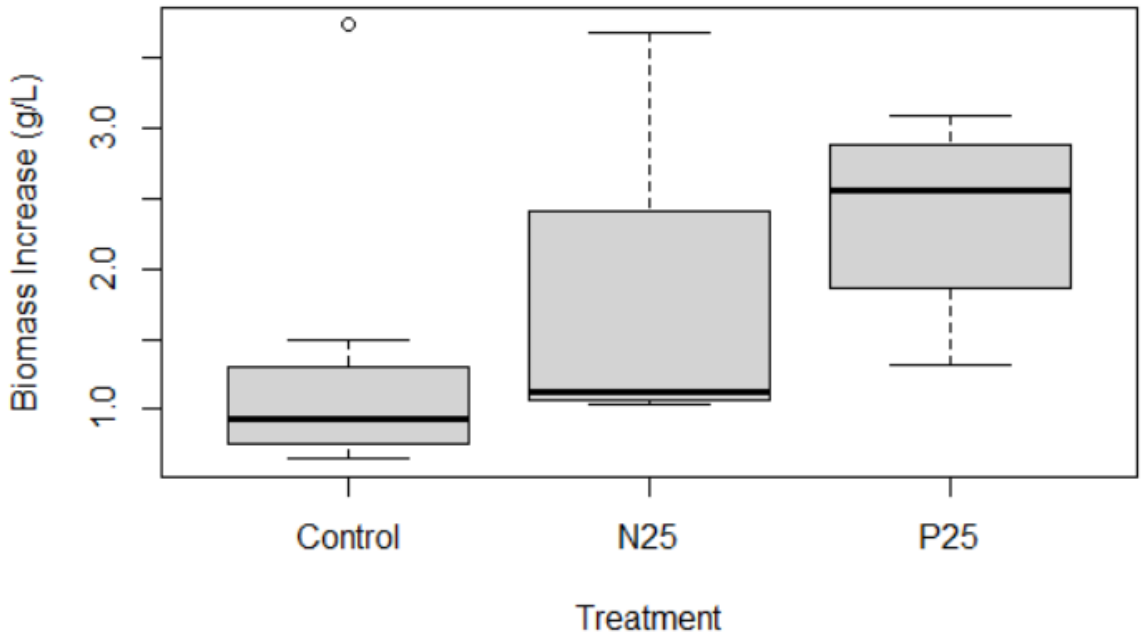

Figure 22 A boxplot comparing the net dry weight increase (in mg/ml) between the different treatments where C = Control; N = N-reduced (25%); P = P-reduced (25%).

Analysis of trimmed data:

With samples 4 and 5 excluded, the result shifted slightly: The P25-treatment was found to be significantly different, with a p = 0.0004 (appendix B, fig. B-17). From the boxplot (fig. 23) it is clear that cultures fed P25 had a higher average dry weight, with a mean around 2.5 mg/ml compared to a mean of ~1.0 mg/ml for control and N-reduced treatments.

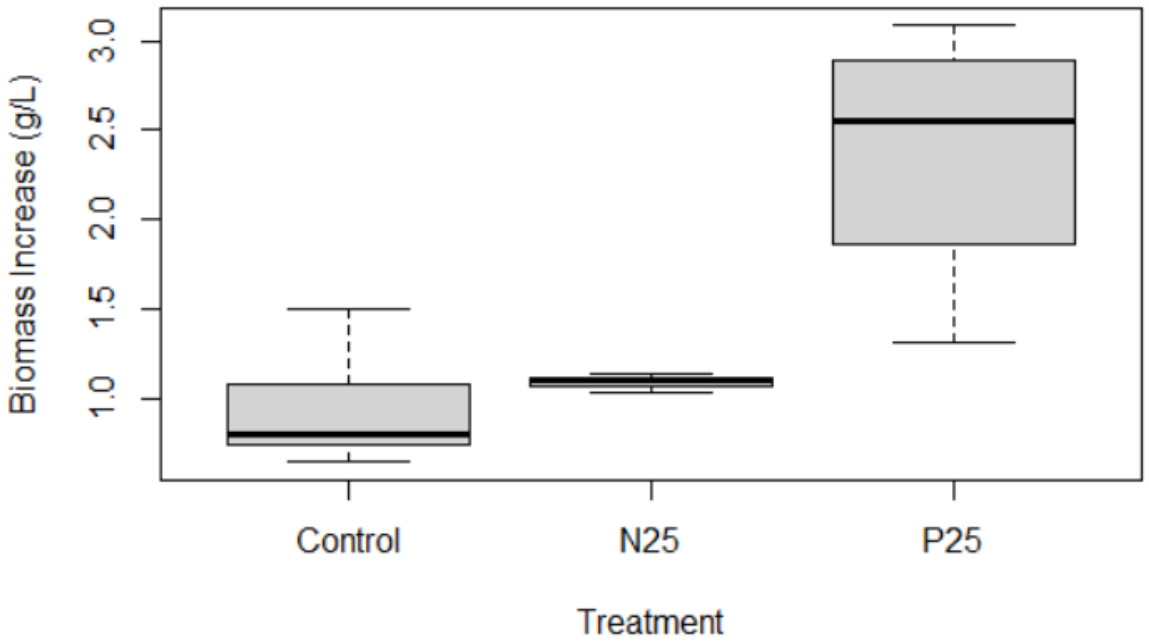

Figure 23 A boxplot comparing the net dry weight increase (in mg/ml) between the different treatments where C = Control; N = N-reduced (25%); P = P-reduced (25%). The data for this boxplot excludes samples 4 and 5 from this run, as done for light absorption (Chapter 3.4.1)

3.5 Fourth continuous ministat test

The fourth continuous cultivation also used media M8 (pH 6.23), N25 (pH 6.26), and P25 (pH 5.91), but had a further increase in flowrate, with the pump speed set to 2.5, estimated to be equivalent to 32mL/day, or a flowrate of 0.71 d^{-1}. This is almost double the theoretical maximum growth rate as obtained in the batch growth (section 3.1). The duration of this experiment was 688h, and stationary phase could in this case not be determined, due to heavy relative fluctuation in optical density of the cultures.

Due to the fluctuation, the graphs can be hard to trace, but they largely follow each other, peaking and stooping around the same time, somewhat rhythmically. The reason for this rhythmic pattern of growth and decline is likely due to sampling error, which will be addressed in the discussion. As can be observed in fig. 24, optical densities (absorbance at 540nm) is a lot lower at 0.71 d^{-1} than at lower dilution rates

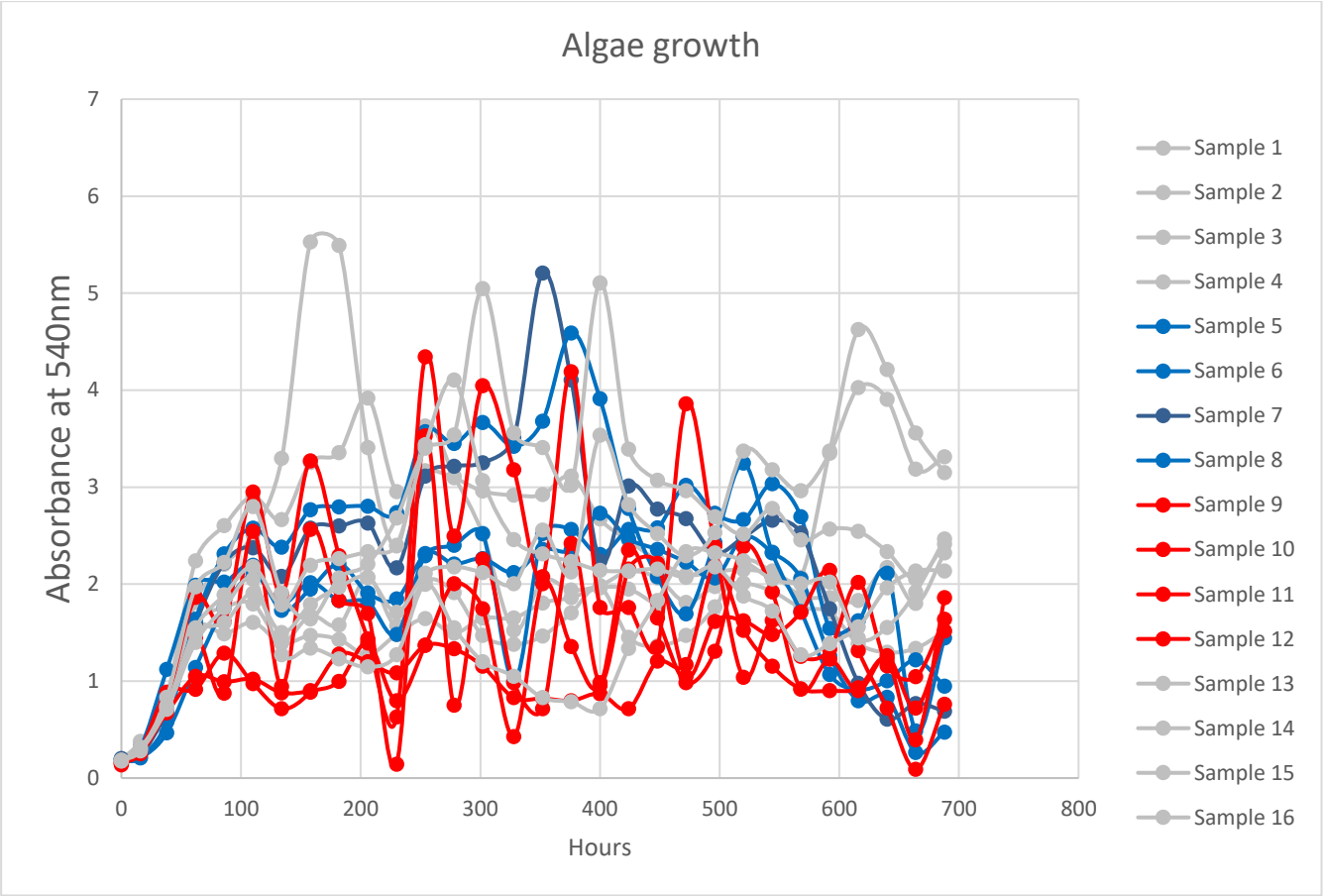

Figure 24 The growth curves, color coded by treatment; Grey samples (1-4, 13-16) represent M8 Control, blue samples (5-8) phosphate-reduced (25%) cultures, red samples (9-12) nitrogen-reduced (25%) cultures. Data in appendix A, table A-10.

There were reoccurring incidents of medium feed-tube blocking, for instance sample 4, which was blocked repeatedly from ~110 h to ~180h, which may account for the large peak (fig. 24). However, the fluctuations are more pronounced in nitrogen-reduced cultures, which becomes apparent when they are removed (fig. 25), and as stated is likely due to sampling error.

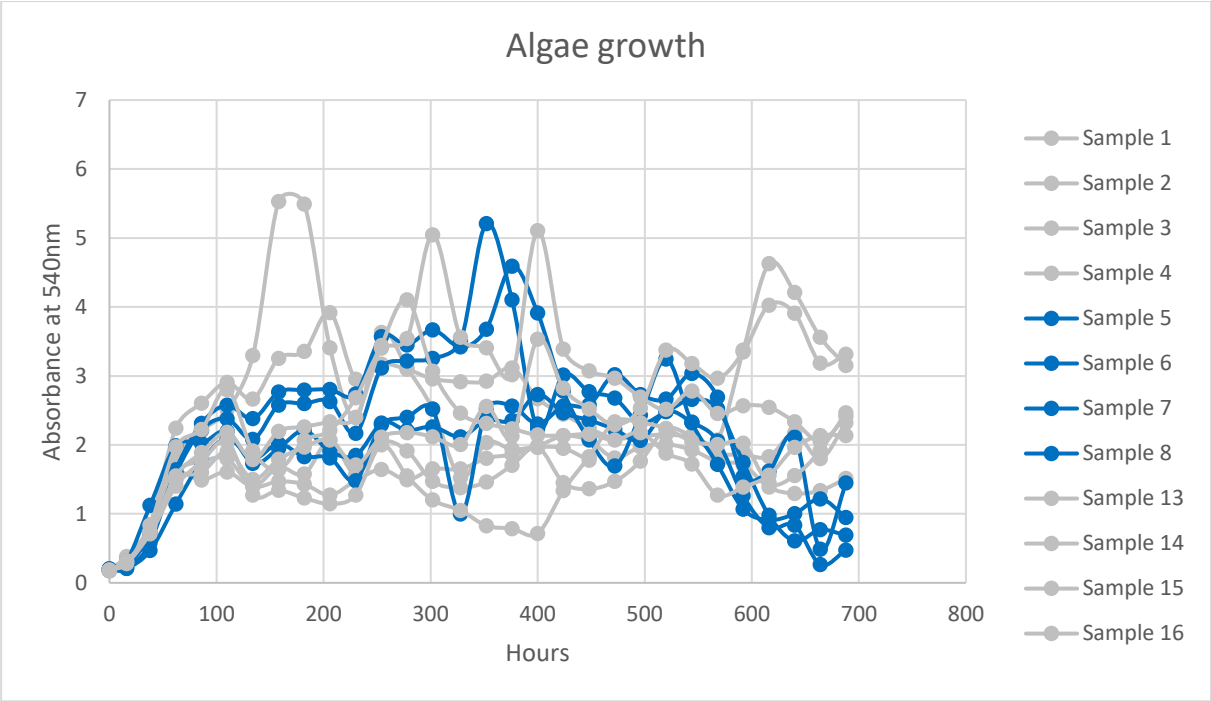

Figure 25 The growth chart of the algae cultures with treatments M8 (grey) and P25 (blue); N25 excluded.

At the final measurement (688H), although the growth curves had been fluctuating, the treatments seem to show a grouping. Throughout the experiment, the curves for the same treatments largely follow each other, and an ANOVA of the OD by treatment group at termination, visualized by the boxplot (fig. 26), revealed significant differences between all treatments. This may suggest that the algae fed control medium were able to cope better with the high rate of flow, and that the stress of flowrate as well as reduced nutrients is hard to handle.

All ANOVA-assumptions met (se appendix B). Levene's test: $p = 0.508$ ($p > 0.05$), variance ratio < 5; and normality of residuals established at $p = 0.290$ ($p > 0.05$).

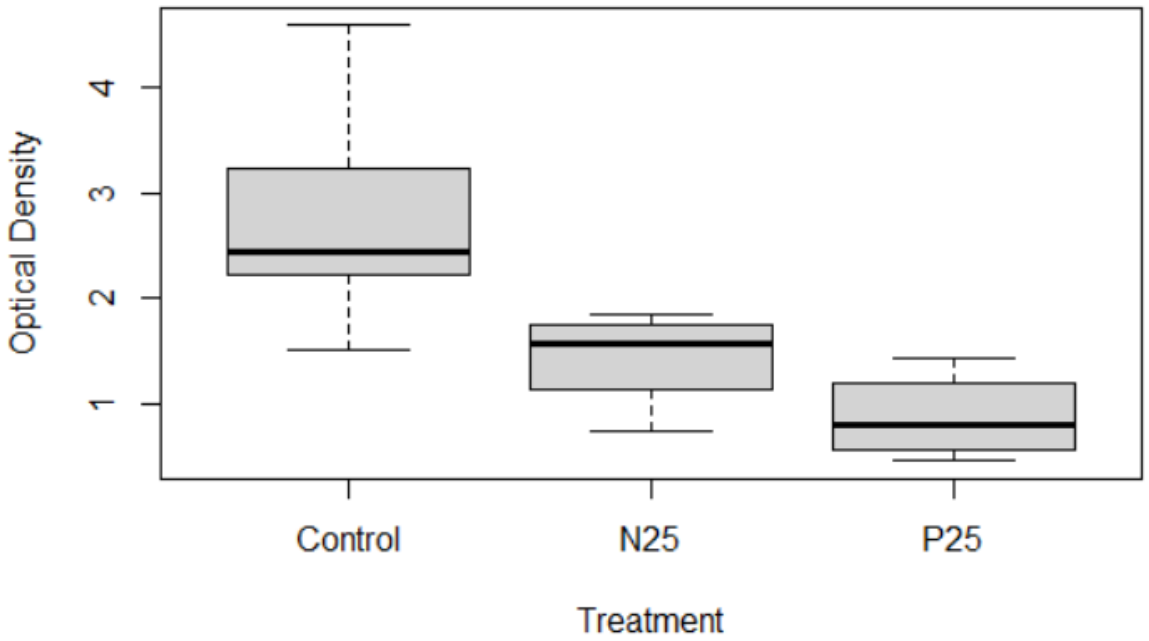

Figure 26 The boxplot compares the means of endpoints (optical density at 688h) by treatment, where N25 = N-reduced (25%); P25 = P-reduced (25%).

3.6 Fifth continuous ministat test

3.6.1 Light absorption

The fifth continuous cultivation was performed testing new media, which except for the control M8 (pH 6.24), included the further reduced N5 (5% nitrogen; pH 6.30), N10 (10% nitrogen; pH 6.32), P5 (5% phosphate; pH 4.55), and P10 (10% phosphate; pH 4.75). The pump speed was again set to 2.5, estimated to be equivalent to 32 mL/day, or a flowrate of 0.71 d^{-1}. The duration of the experiment was 394 hours. Again, stationary phase was hard to determine due to fluctuation.

In this experiment, even lower concentrations of nutrients were introduced, down from 25%, to 5% and 10%. The experiment was intense, with highly reduced nutrient concentrations, and a high medium turnover rate. As can be observed in the growth chart (fig. 27), optical densities (absorbance at 540nm) is a lot lower at 0.71 d^{-1} than at lower dilution rates.

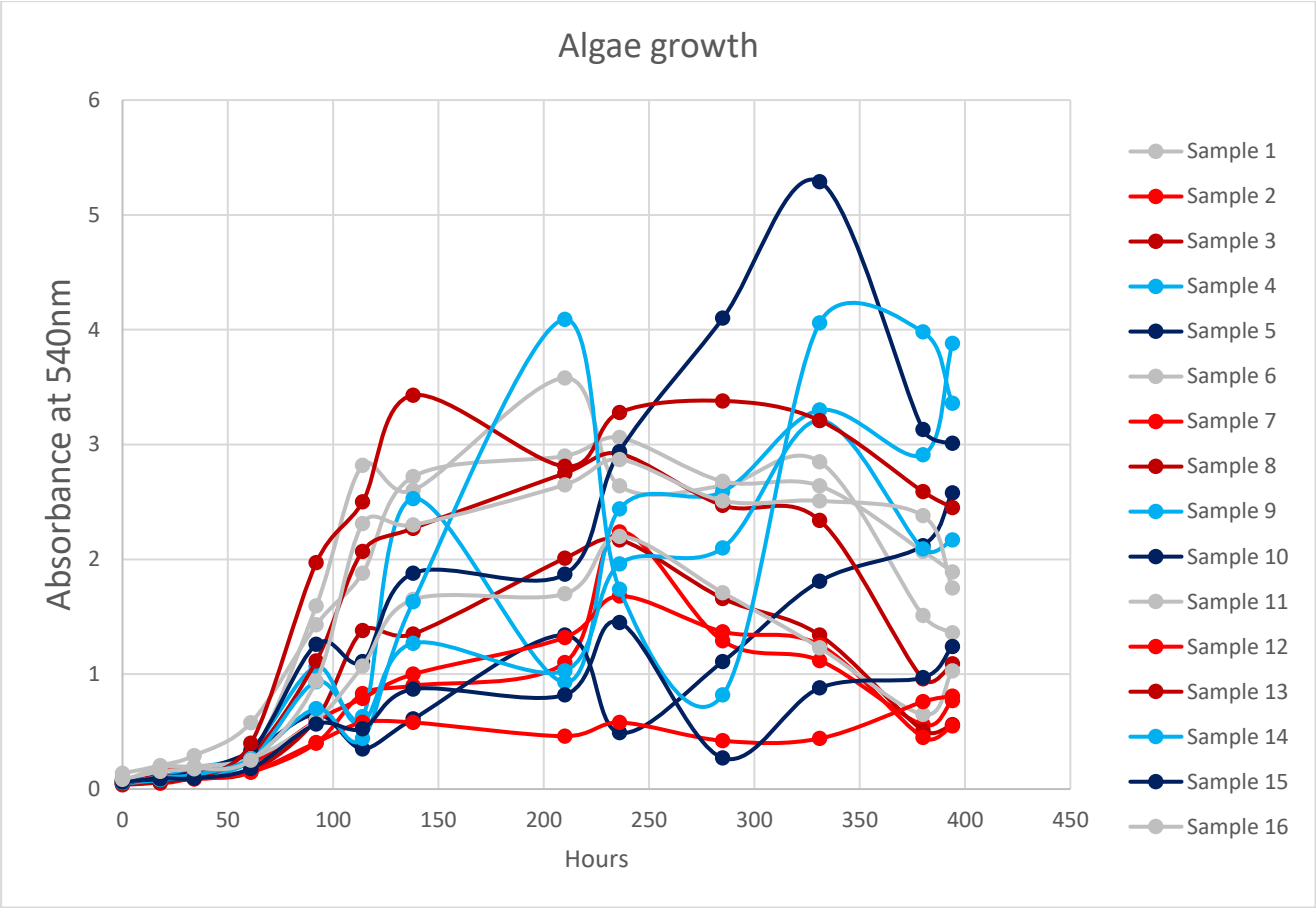

Figure 27 The growth curves of the individual ministats, color coded by treatment; Grey samples (1, 6, 11, 16) represent M8 Control, red samples (2, 7, 12) nitrogen-reduced (5%) cultures, dark red (3, 8, 13) nitrogen-reduced (10%) cultures, light blue samples (4, 9, 14) phosphate-reduced (5%) cultures, dark blue (5, 10, 15) phosphate-reduced (10%) cultures. Data in appendix A, table A-11.

At final measurement (394h), it seems from the boxplot (fig. 28) that P-reduced medium fared a little better than both the control and N-reduced medium, and indeed ANOVA revealed no significant differences with the exception of the 5% phosphate-treatment, which surprisingly grew better than all the other treatments. Throughout the experiment, there was intermittent blocking of medium feed-tubes, causing some sudden increasing in culture density (notably sample 10 spiking to OD > 5 around 300 hours).

The assumptions for ANOVA were met (Levene's test returned $p = 0.620$; Shapiro-Wilks returned $p = 0.816$; appendix B). However, a variance ratio of 48.49 (appendix B) indicates the variance is too high.

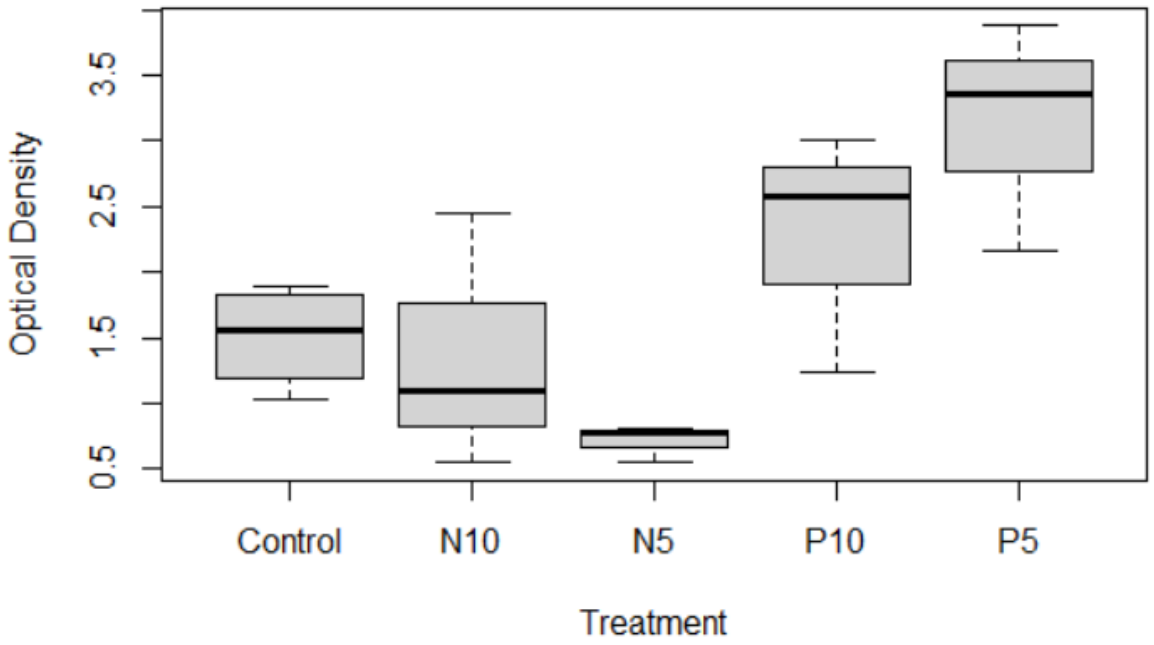

Figure 28 The boxplot compares the means of endpoints (optical density at 394H) by treatment, where N10 = N-reduced (10%); N5 = N-reduced (5%); P10 = P-reduced (10%), P = P-reduced (5%).

A type-III ANOVA was performed (see appendix B) to account for unequal variance, finding that there were significant differences by the different treatments, although it seems likely this is due to random chance as a product of a rate of flow. The fact that most of the treatments do not differ significantly indicates that the high rate of dilution has the biggest impact on their ability to grow.

No outliers were found in this dataset (See appendix B, fig. B-24).

3.6.2 Dry weights

Samples from the individual cultures were harvested at inoculation (0h) and termination (394h), and the dry weight measured. The dry weight for each sample can be seen in fig. 29, and the net growth (weight at termination minus the weight at inoculation) per treatment in fig. 30. An ANOVA was performed, returning no significant differences between treatments, except for P5 (5% phosphate), at p = 0.0268 (appendix B, fig. B-25). Assumptions for ANOVA were met (appendix B, fig. B-26). The dry weights per treatment averaged between 1-2.5mg/ml.

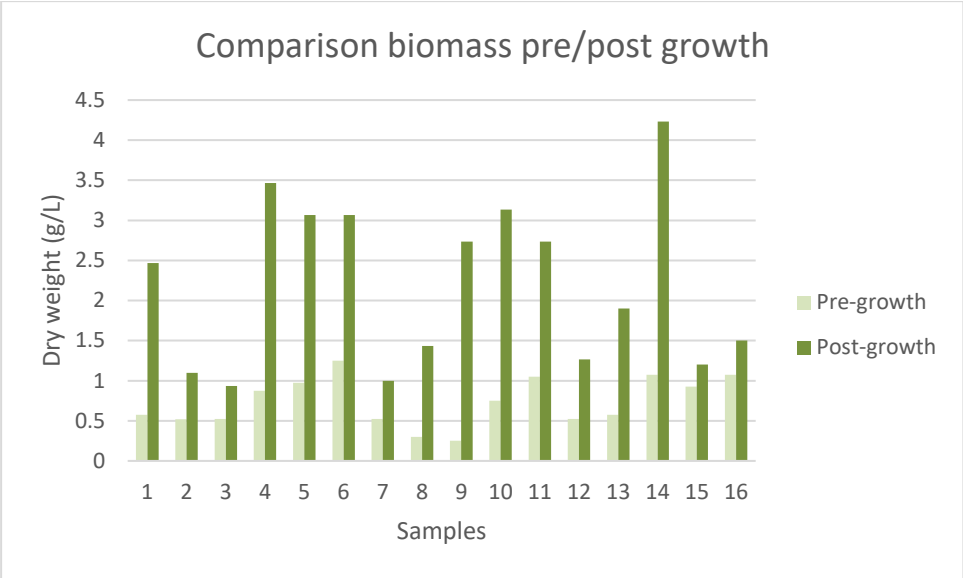

Figure 29 A bar chart showing the total growth of all samples at 0h and 394h. Biomass expressed in g/L. Data in appendix A, tables A-12 and A-13.

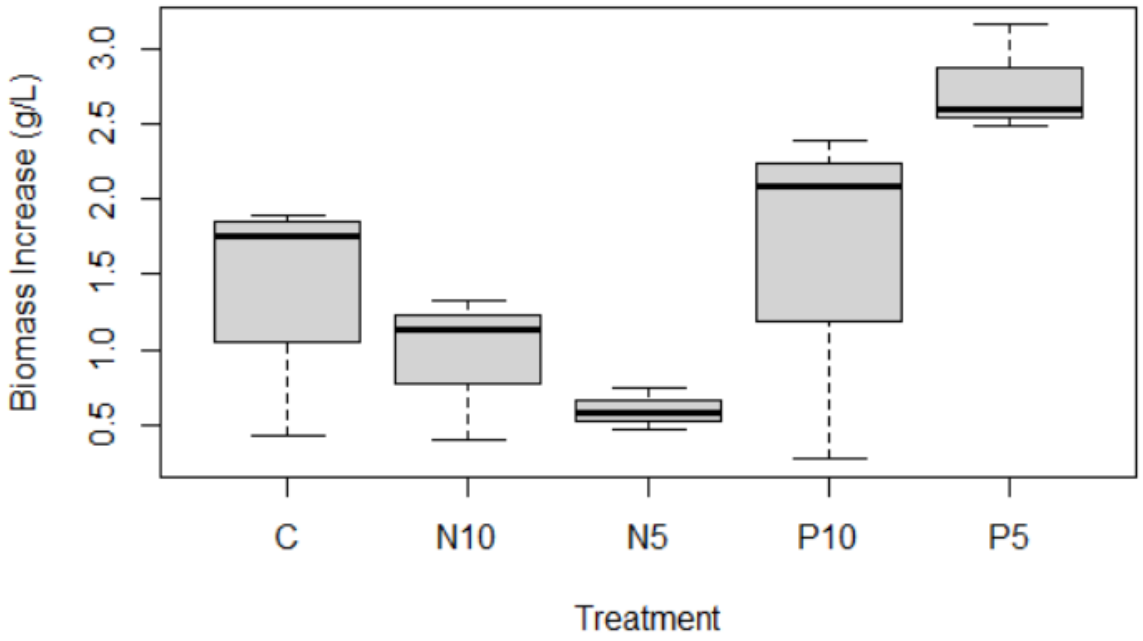

Figure 30 The boxplot compares the means of endpoints (net growth of dry weight, in mg/ml at 394h) by treatment, where C = Control; N10 = N-reduced (10%); N5 = N-reduced (5%); P10 = P-reduced (10%), P = P-reduced (5%).

Although assumptions were normal, the variance ratio between minimum and maximum net growth was very high – 72.3, likely as a result of the low values for certain samples (sample 15 (treatment P10) at extreme low, with a net growth of 0.275 mg/ml; sample 14 (treatment P5) at the other extreme with a net growth of 3.158 mg/ml)

3.7 Sixth continuous ministat test

3.7.1 Light absorption

The sixth continuous cultivation, performed with media M8 (pH 6.23), N5 (pH 6.27), N10 (pH 6.26), P5 (pH 4.64), and P10 (pH 4.73), and cultures inoculated with algae which had been cultivated in the chemostat conditions for one week before inoculation, differing from the other cultivation tests, which were all inoculated with naïve algae, as stated in materials and methods (section 2.1; Model organism), the idea being to test whether the algae showed any signs of acclimatizing.

Pump speed was set to 2.5, estimated to be equivalent to 32 mL/day, or a flowrate of 0.71 d^{-1}. The duration of the experiment was 327 hours, with stationary phase determined to occur around 231 hours. This was a repeat of the conditions of the previous run, with a high medium turnover rate, and very low nutrient concentrations. As can be observed from the growth chart (fig. 31), there was less fluctuation in growth this time.

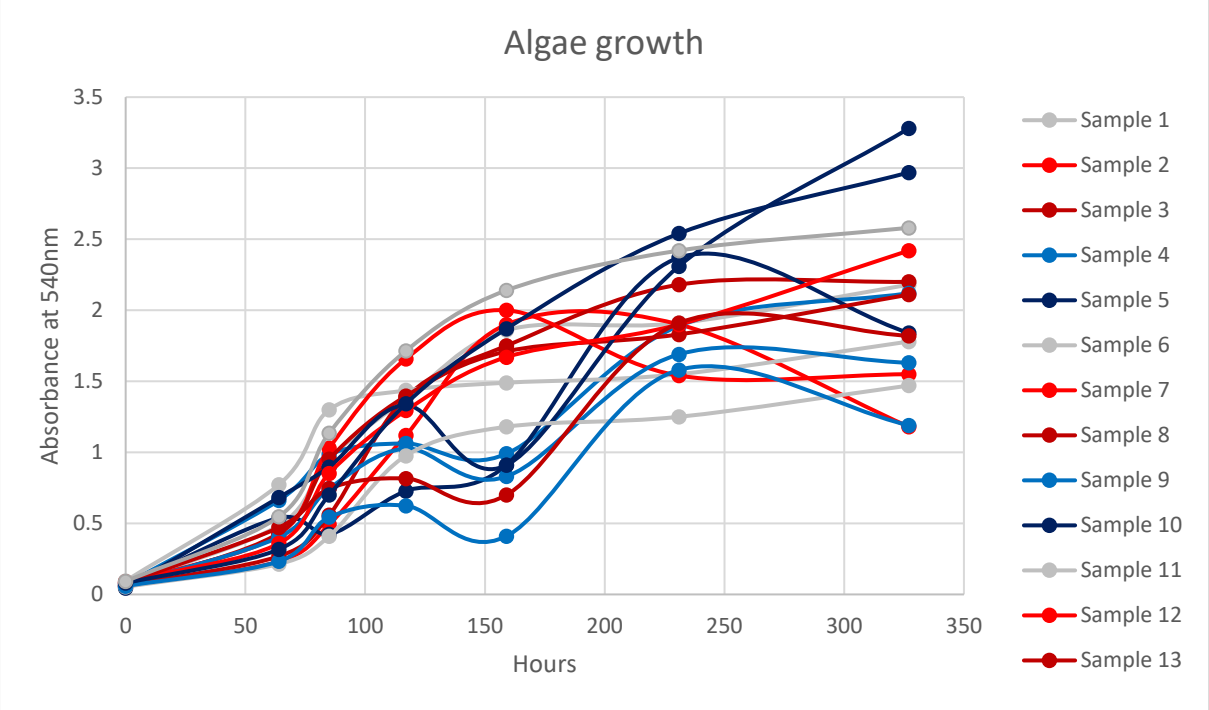

Figure 31 The growth curves of the individual cultures of chemostat tubes, color coded by treatment; Grey samples (1, 6, 11, 16) represent M8 Control, red samples (2, 7, 12) nitrogen-reduced (5%) cultures, dark red (3, 8, 13) nitrogen-reduced (10%) cultures, light blue samples (4, 9, 14) phosphate-reduced (5%) cultures, dark blue (5, 10, 15) phosphate-reduced (10%) cultures.. Data in appendix A, table A-14.

ANOVA indicated no significant differences between the different treatments, and when inspecting the boxplot visualizing differences in OD between treatments (fig. 32), this is apparent as well. The optical density of the cultures (absorbance at 540nm) is at this point

very low, so although the boxplot may seem to show differences in means, ANOVA indicates that these are minimal and insignificant.

The ANOVA assumptions were met with Levene's test returning $p = 0.778$, and Shapiro-Wilks returned $p = 0.778$ as well, both well above $p > 0.05$ for equal variance and normal distribution, respectively. However, the ratio between maximum and minimum variance was 14.57, which is quite high. Therefore a type-III ANOVA was performed, but returned no significant differences between treatment groups.

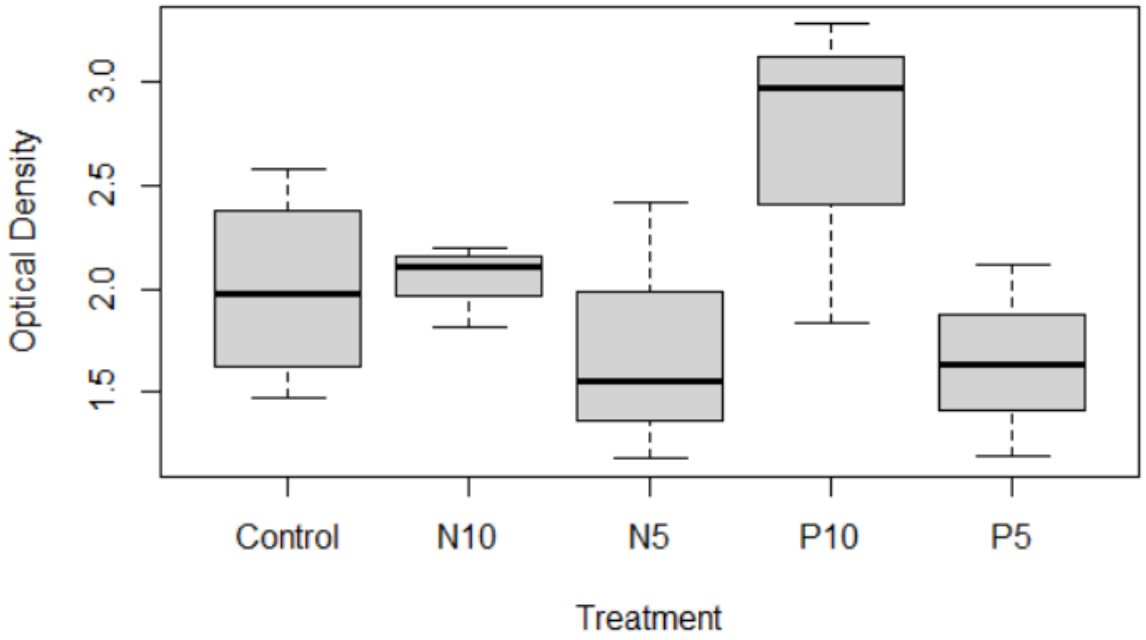

Figure 32 The boxplot compares the means of endpoints (optical density at 394h) by treatment, where N10 = N-reduced (10%); N5 = N-reduced (5%); P10 = P-reduced (10%), P = P-reduced (5%).

3.7.2 Dry weights

Samples from the individual cultures were harvested at inoculation (0h) and termination (327h), and the dry weight measured. The dry weight for each sample can be seen in fig. 33, and the net growth (weight at termination minus the weight at inoculation) per treatment in fig. 34. An ANOVA was performed (appendix B, fig. B-25), returning no significant differences between treatments, except for P5 (5% phosphate) at $p = 0.0317$. Assumptions for ANOVA were met (appendix B, fig. B-26). The dry weights per treatment averaged between 1-2.5mg/ml.

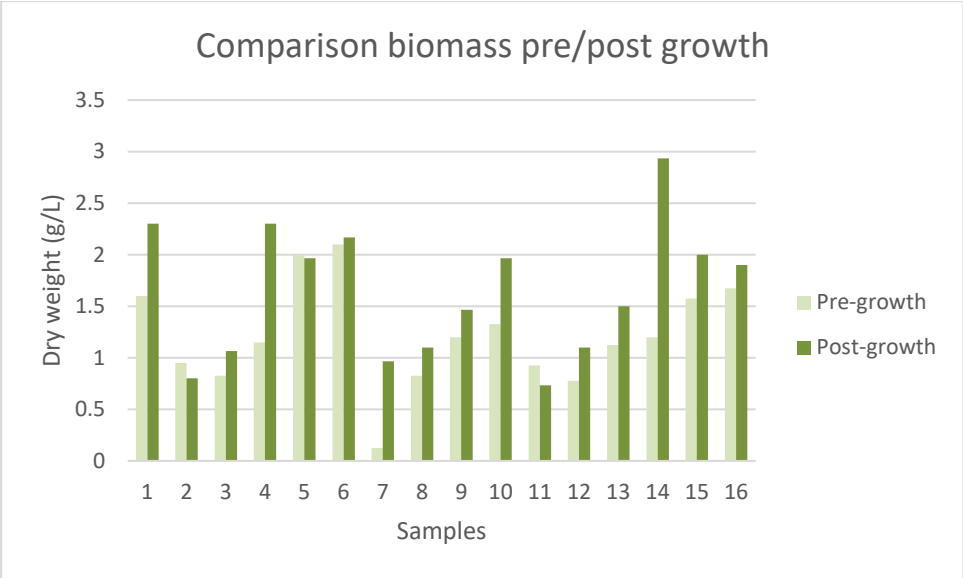

Figure 33 A bar chart showing the total growth of all samples at 0h and 327h. Weight expressed in g/L. Data in appendix A, table A-15 and A-16.

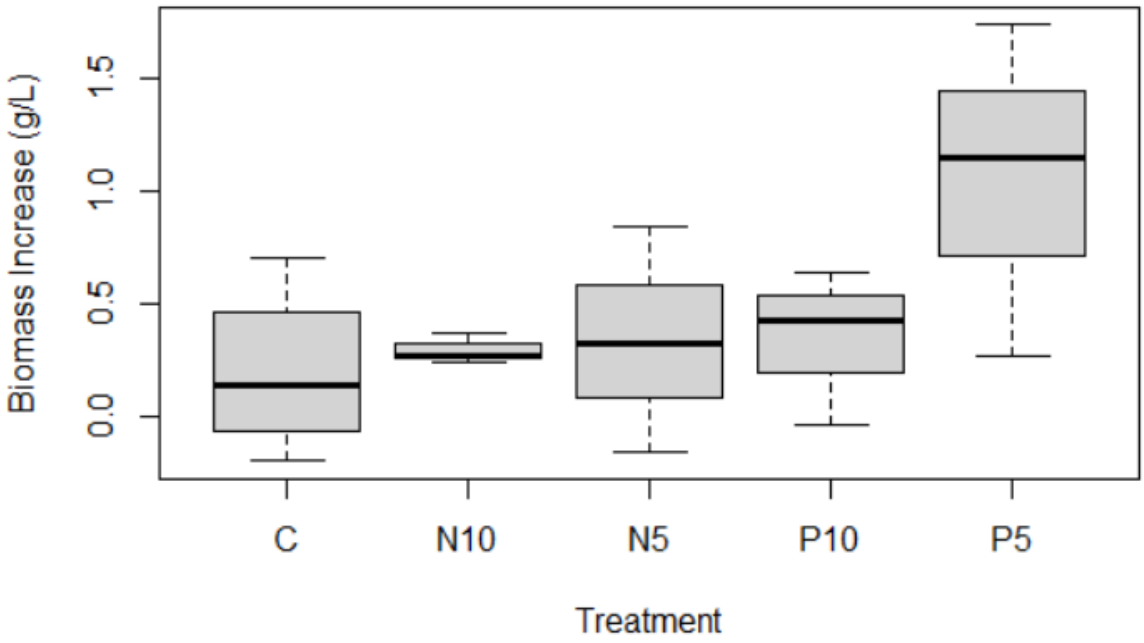

Figure 34 The boxplot compares the means of endpoints (net growth of dry weight, in g/L at 327h) by treatment, where C = Control; N10 = N-reduced (10%); N5 = N-reduced (5%); P10 = P-reduced (10%), P = P-reduced (5%).

3.8 Comparison of culture growth and flowrate

The data points were gathered across all continuous runs, and optical density (absorbance at 540nm) as a function of medium flow was graphed (fig. 35). ANOVA returned significant differences for the different flowrates, but the assumptions for ANOVA were not met (unequal variance at p = 9.77e-06; abnormal distribution at p = 6.225e-06), which can be expected due to the unequal conditions of the different flowrates, and the variations arising in OD as a consequence. However, the data show a clear inverse relationship between optical density and flowrate, which indicates that higher flowrates, the algae have a hard time growing fast enough to maintain a high culture density.

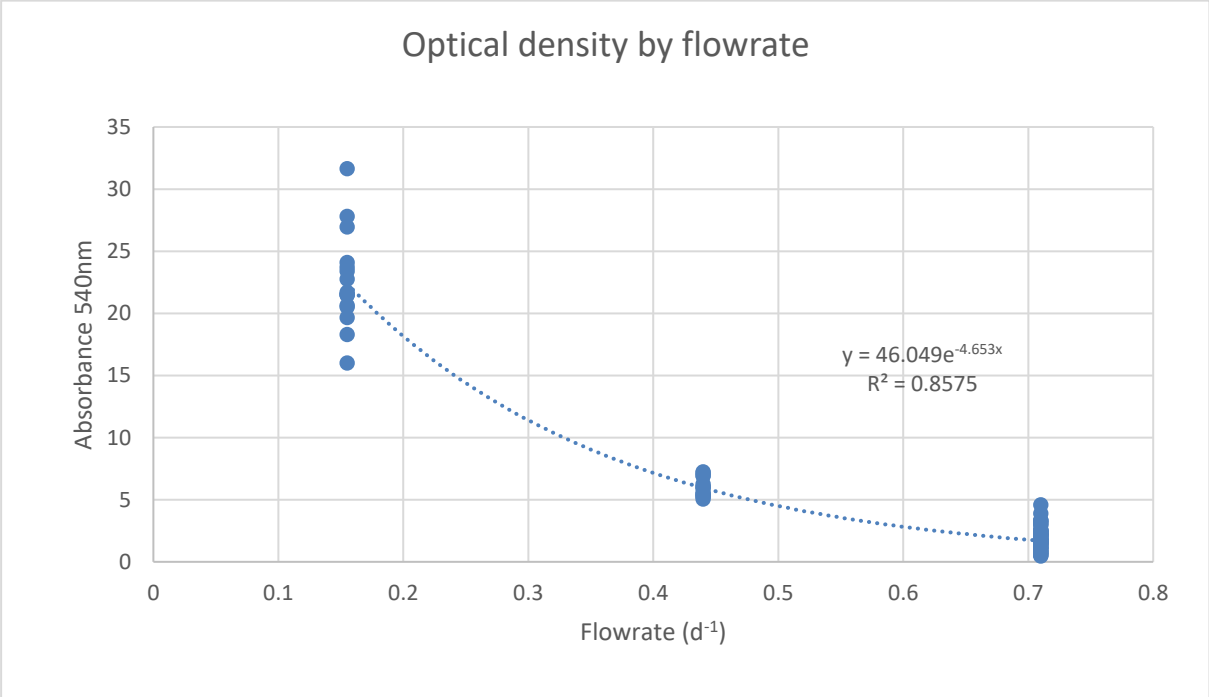

Figure 35 A scatterplot of the optical densities (light absorption at 540nm) as a function of dilution rate.

3.9 Stir tube cultivation test

The stir tube experiment was performed once and without replicates, to test whether it would work for the small scale of the mini-chemostat array. It seemed to reach a steady state around 214h (OD 32.9) (fig. 36), which is both quite rapid and quite dense. The medium used was M8 control, and dilution rate was set at 0.5 rpm (0.155 d^{-1}). The same dilution rate used for the first and second continuous runs. The stir tube comparatively outgrew the normal continuous cultivation experiments at the same flowrate, reaching higher optical densities (the stir tube growing to OD 32.9 at 214h, with runs one and two growing to OD 23.9, and 21.0 in the same time, respectively), ending up with a shorter time to reach the stationary phase, than the first continuous run also.

In other words, the stir tube culture not only grew well, but comparatively faster and denser than the normal treatments.

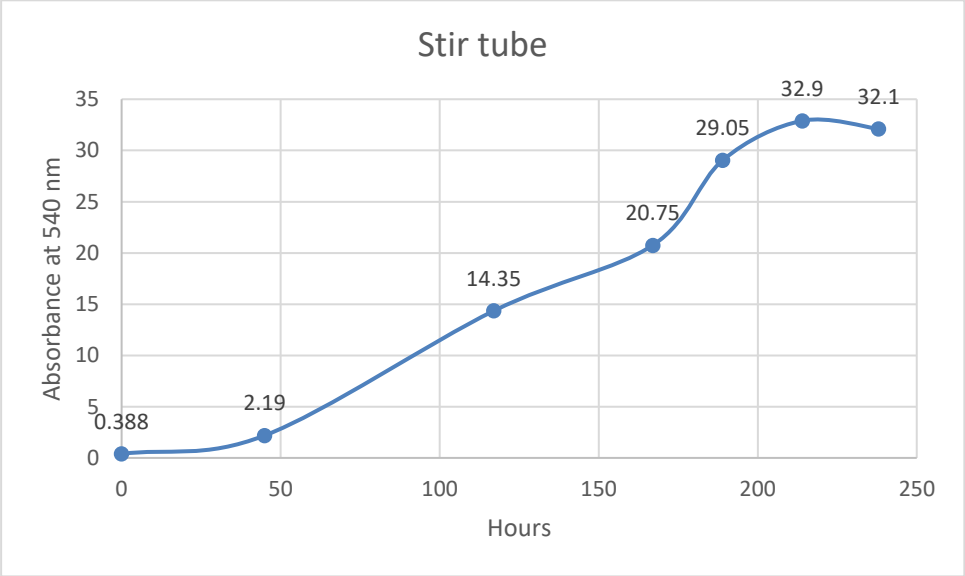

Figure 36 The growth curve of the stir-tube experiment, terminated at 238h

4 Discussion

4.1 Findings

The purpose of this work has been to design and test an efficient mini-chemostat system for scientific research which could allow for the rapid growth and adaption of microalgae under exposure to stress conditions, intended to provoke phenotypical and genotypic changes towards a desired trait. This work demonstrated the basic functionality of the ministat system for microalgae, and by comparing with similar studies in other microorganisms, an argument will be made for how this concept can be further developed, refined, and ultimately utilized as a tool in research or industry. As the discussion will touch on many topics, it will be organized in the following way: First, the results will be discussed, then the mechanical issues will be addressed, then biological issues, then the analytical tools, before finally summing up how an improved version of this system ideally would look.

During the course of the experiments, three different pump speeds (and thus, dilution rates) were used, these were 0.5rpm, 1.5rpm, and 2.5rpm of the rolling pump, equaling $0.155d^{-1}$, $0.44d^{-1}$, and $0.71d^{-1}$, respectively. The first and second runs operated at 0.5 rpm, the third run at 1.5 rpm, and the fourth, fifth and sixth run were operated at 2.5 rpm. This was shown to be the determining factor (see fig. 35 in section 3.8 (Results)) for growth rate, with the growth parameters of the cultures reducing drastically as pump speed was increased. How each treatment performs is thus best compared in relation to the others at the same pump speed, rather than comparing growth parameters across runs at different pump speeds.

The first continuous cultivation had few replicates, but demonstrated that the system was able to function as intended. The microalgae grew well, and showed a clear stationary phase after around 200 hours, a growth rate which exceeded that of the baseline demonstrated during the batch growth (section 3.1), showing a growth curve typical for continuous cultivation (section 1.2, fig 2). The cultivation was considered a success, demonstrating the functionality of the system.

The second continuous cultivation was performed with all 16 ministats and different treatments, using the media M8, N25, and P25. The cultures grew well, and treatment differences were pronounced during the growth phase, with N25 and P25 growing faster than the control until stationary phase. This state of affairs did not last, however, as N25-cultures

had lower optical densities than both M8 and P25, and were visibly paler than the other cultures, which is likely a symptom of nitrogen-deficiency called “degreening” (Chu et al., 2015). Nitrogen deficiency is likely to lead to reduced cell division, and thus, reduced growth in general (Chu et al., 2015). Indeed, cell count were almost half that of the other cultures (table A-5, appendix A), but biomass, although lower, was not significantly lower than the other treatments (Section 3.3.2, fig. 16).

The third continuous cultivation had an increase in pump speed, where dilution rate was set to approximate the unconstrained growth rate (between 0.36 and 0.384 d^{-1}) discovered during batch growth (section 3.1). As there was repeated blocking of medium feed-tubes, and consequently artificially dense cultures, two observations were removed after statistical analysis had confirmed them as outliers. Other cultures were occasionally blocked as well, a problem which seemed to increase with medium inflow rate. The cultures grew well, but reached much lower concentrations than previous runs, an effect of the flowrate. At termination, the treatments were not found to have significant differences in terms of optical density, but cultures fed P25 had grown a little denser overall, a difference which was shown to be significant when measuring biomass. It seems from this that flowrate was the dominating factor in limiting growth, but it is surprising to note that P25, a reduced medium, performed so well. It has been found that phosphorous-reduction does not impact biomass accumulation to the same degree as does nitrogen-reduction (Kumari et al., 2021), but control is expected to perform better than a reduced medium.

The fourth continuous cultivation was performed at the highest flowrate (0.71 d^{-1}), and was characterized by heavy relative fluctuation in optical density during growth (section 3.5, fig. 24), but upon inspection it became clear that this was mostly in the nitrogen-reduced cultures (section 3.5 fig. 25), and can likely be explained by the following: The nitrogen-reduced cultures had a tendency to settle at the bottom of the ministat, thus there was a heavy gradient of culture density for the N25 treatment, which would require manual stirring to ameliorate. This experiment was performed during COVID-lockdown, and access to the lab was given to limited staff only, and as such, samples were taken by another operator. It seems likely that the cultures were not re-suspended before sampling, as the growth curves seem to fluctuate rhythmically, and a suggestion here is either that the cultures were intentionally stirred *after* sampling, or that the cultures were stirred by accident when the silicone cap was placed back after sampling, which would have caused the gas supply rod to scrape along the bottom of the

vessel, and clots of algae to float up and be dispersed by the bubbling action. The resulting growth curves could therefore be misleading. This is supported by the grouping of the treatments at the termination of the experiment, which found that culture densities were significantly different between treatments.

The fifth continuous cultivation, also performed at the highest flowrate (0.71 d^{-1}), and further reduced media (down to 10% and 5% nutrient concentrations) were tested. This was to assess whether more dramatic differences would manifest between treatments. The effects were likely somewhat reduced by the high flowrate, with both the control and nitrogen-reduced media performing worse than phosphate-reduced media, both in terms of optical density (section 3.6.1, fig. 27), and biomass (section 3.6.2, fig. 28). The treatment with the lowest phosphate content, P5, was found to grow significantly denser and have higher biomass than all other treatments; but at this rate of flow it should be mentioned that values for optical density, as well as biomass, are quite low, and the differences could be due to chance.

Before the sixth continuous cultivation, the algae were given a week to acclimatize to the conditions before being re-inoculated, which can perhaps explain why the growth curves seem to be more consistent (section 3.7.1, fig. 31). The implementation of filtered media also helped with consistency, as there was no blocking of tubes during this cultivation. Statistical analysis revealed no significant differences, again with the exception of the P5-treatment, which had a higher biomass than the other treatments (section 3.7.2, fig. 34).

Finally, the implementation of a stir tube was performed to test the concept for the improved version, as it would prevent the cultures from settling, and help in mixing the cultures better. The culture grew fast and dense, no problems were encountered, the algae growing well with the magnet in the culture, seemingly not suffering any adverse consequences from the kinetic action or contamination. The stir tube test was thus considered a successful demonstration of a stir tube prototype.

From the data gathered across the different cultivations, it is apparent that dilution rate should be kept below maximum intrinsic growth rate, as it would result in more pronounced differences between treatment, and make elucidating phenomena such as phosphate-reduced treatment seemingly growing better than the other treatments easier, the lower flowrate allowing for higher culture densities in general, which could perhaps show the phosphate-

reduced treatments abilities to persevere to be a fluke due to low densities and random chance. It may also be the case that acclimate the algae to the cultivation conditions before starting data gathering reduces noise and fluctuation, as it has been demonstrated to reduce lag time in other studies (Japar et al., 2021). By acclimation is meant cultivating the algae for a period in the system under the conditions to be investigated, before sampling and starting a fresh cultivation using the acclimated algae.

4.2 System issues

As stated in Materials and Methods (Section 2.6 Design of Chemostat setup) and results (Section 3) some problems were encountered during the experimental stage of this project. It should be noted that the system is completely "home-made", using standard lab equipment, and some more expensive parts such as the peristaltic pump and the gas mixing system. Although based on similar solutions (Takahashi et al., 2014; Skelding et al., 2018), this improvised setup did differ in several aspects such as medium delivery (Takahashi et al. (2014) and Skelding et al. (2018) using a computer-controlled needle-pump), which in the case of this experiment was analogue; the same is true for the mixing, which was achieved by aeration rather than magnetic stirrers, nor were there any optical sensors. In other words, no smart technology or feedback-systems other than mechanics and physics was used to operate it.

The analogue nature of the system means that features such as integrated temperature control is non-existent, relying on ambient temperature during operation. The same is true for lighting, the system being dependent on external light such as sunlight or as in the case of the setup of this project, a lamp fitting the width of the system, for growth. As this project utilized the mesophilic *C. vulgaris*, the setup could be left in room temperature and the cultures grow well; ideally this setup can be adapted for any microalgae, though, which would mean an integrated temperature- and light control should be included for the improved version.

There were issues both with the system itself, as well as with the analytical tools (most notably the Multisizer, mentioned in section 2.6), but the focus will be on the issues pertaining to the system, which will form the foundation for suggested improvements for the improved design. Having now outlined the general setup, the issues will be discussed in detail.

The commonest problem encountered during operation of the system, was blockage of tubing leading medium to the ministats. This would mostly occur in the pump-tubing, specifically at the end of the tubing where a needle would connect the pump-tube with the silicone tube feeding into the ministat. Smooth operation of the system therefore required a lot of maintenance due to the frequent and repeated blockage, often causing differences in inflow and consequently algae growth (as noted in results, sections 3.4 to 3.6). Blocking was a source of frustration and disruption of continuous and consistent data generation, although the high number of replicates proved valuable in balancing out noise in the data.

To remedy frequent blocking, the medium was filtered after autoclaving to reduce the amount of undissolved matter (implemented from fifth continuous cultivation, section 3.6), and this did reduce frequency of blocking, but did not stop the problem entirely. This could be due to some component of the medium undergoing precipitation, as indeed the problem was found to occur mostly after some days of the medium reservoir standing stagnant besides the setup. Another effort to prevent blocking was to lift feeding tubes higher in the reservoir tank, so as to avoid intake from the bottom of the reservoir, where the precipitate would accumulate. Interestingly, precipitation seemed to occur more often with the nitrogen-reduced medium, indicating that perhaps an imbalance in pH would exacerbate precipitation. This is, however, somewhat confusing, as the suspected chemical forming the precipitate was KNO_3, which is the nitrogen source (of which there is less in the nitrogen-reduced medium), and the pH of nitrogen-reduced media were fairly similar to M8 control (see results, sections 3.2-3.7).

Blocking of medium supply resulted in a reduction of culture volumes in the affected ministats, but the effects would vary with the duration of blockage, and differences would not be pronounced if they were remedied in a timely manner, not more than 12 hours. A related issue is the fact that medium is fed through individual tubes (in addition to the individual tubes feeding the gas-mixture, as well as the tubes for effluent culture); this can easily become tangled and chaotic, and requires a tidy workspace and an organized operator. Color coding and grouping of tubes can be a good, low-tech way of keeping order around the system, but for an improved version, a better system for the tubing will be suggested.

Another problem encountered, often in conjunction with blockage of medium supply, was pressure differences arising in the ministats, which, relying on a single source of gas dispersed

into each chemostat by a divider (i.e. no smart-control, or individual pump leading gas in) would result in gas not entering a ministat at all, rather following paths of least resistance to other tubes, which can have a knock-on effect on the other ministats: When the pressure drops in one or more ministats, the pressure will increase in all the remaining ones; this might lead to the silicone cap of any ministat to pop open with pressure, which further reduces resistance, and results in even more gas escaping there, reducing the overall gas supply to the remaining ministats. This is critical for several reasons: In general, there is less CO_2 supplied to the individual ministat; further, the gas input is the main method of mixing, which is important not just for aeration, but also for a homogeneous distribution of nutrients, light exposure, as well as in preventing biofilm-formation, with algae clinging to the side and bottom of the glass tubes.

Fine adjustments to the gas-disperser would improve the problem, as well ensuring a good seal of the silicone cap, and increasing the effect of the aquarium pump delivering air, as this was the main driver of the gas supply, the CO_2 supply not being strong enough to drive mixing on its own. In addition to this, it was found that decreasing the volume of the humidifier from 2L to 1L would increase overall gas pressure to the system, without any obvious effect on gas humidity as no increase in evaporation was observed.

Finally, the roller pump would sometimes “chew up” the pump tubing, ripping the tubing through the pump and dramatically disrupting medium supply. This was a problem not just for the tubes which were dragged through the pump, but also because the under-pressure created by the pumping action would siphon the medium from the reservoir onto the ground; this thankfully didn’t result in any damage to the pump, but emptying the medium reservoir is a critical error in system design.

4.3 Biological issues

Nitrogen-reduced treatments had a tendency to settle on the bottom of the chemostat, the reason for this is unknown; speculations included nutrient deficiency or a result of pH – however, pH of nitrogen-reduced treatments were consistently found to be roughly equal to the control medium, with phosphate reduced treatments being somewhat lower (Control and N-reduced media normally having a pH 6.2, and P-reduced pH 6.0 or lower). The nitrogen-reduced cultures also tended to be a paler shade of green, and grow less dense in general, symptoms of nitrogen-deficiency.

The medium composition reduction was intended to emphasize the differences in growth, perhaps even establish a critical level of nitrogen starvation, but the results were unclear due to high flowrate. In general, the high flowrate for the last three experiments made the data very stochastic, and the results unreliable, although a growth pattern could be observed, where control-treatments grew well, and nitrogen-reduction impeding growth. It would be interesting to see the effect on lipid composition of the phosphate-reduced treatments, as this might have shed light on the biochemistry behind the perceived better growth rate.

4.4 Analytical tools

In general, the analytical parts of the experiments went well and without any issues besides the Multisizer cell-counter, which stopped working. This effectively left the data gathering relying on biomass and optical density to determine growth, which is unfortunate, but not critical. Determination of biomass and optical density were easy to perform and were done regularly, the only issue in connection with these are that the system does not have a good way of extracting culture for analysis, which means that when it is to be performed (which, in the case of optical density, was either daily or every other day), the operator would have to remove the silicone cap and draw culture out directly from the chemostat with a pipette; this is sub-optimal with regards to preventing contamination of the cultures, and as a minimum it is requires wearing gloves and changing the pipette tip for each chemostat. The volume extracted for optical density was 1mL, which would be quickly replenished and have little effect on the culture, for biomass determination the volume extracted was typically 3-5ml, still with little observable effect on the culture.

4.5 Improving the mini-chemostat array

The improved mini-chemostat array could be made to be more compact in size, so it could more easily fit in for instance a cultivation cabinet, or just to take up less space in general (it need not be as long as the one used for this project). A suggestion for a more compact base is visualized below (fig. 37).

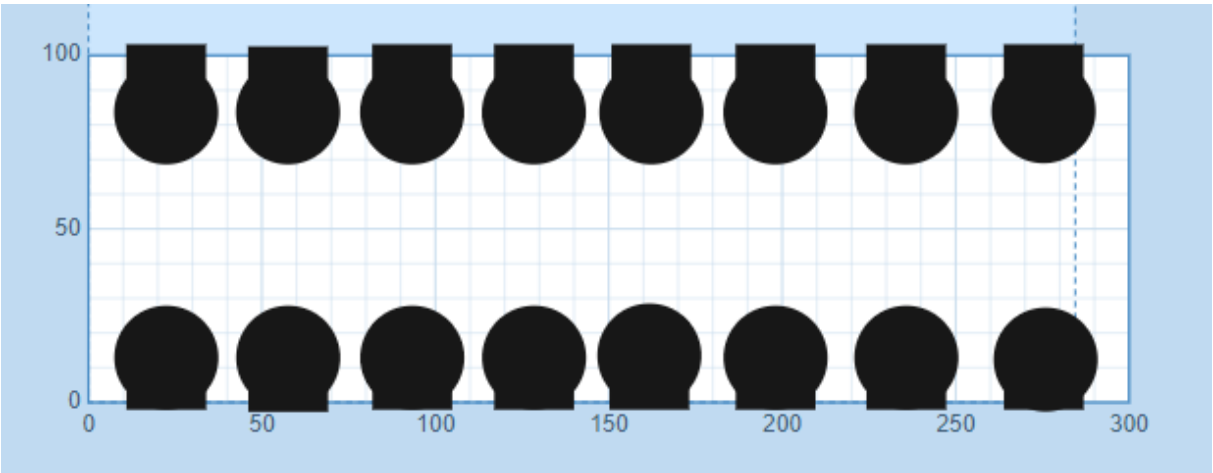

Figure 37 A schematic of the suggested mini-chemostat array Mark 2 (dimensions W300xL100 mm), with 8 wells for growth tube on each side and a slot for LED-light strips; created with Easel Free CNC by Inventables

Further, medium feed-tube and pump tubing diameters should be increased to prevent blocking, and medium should be filtered as a rule; alternately, medium tubing could also be made rigid, as suggested by Skelding et al. (2018). Gas supply needs a tighter, individual control, which would improve upon the static metal divider with spigots. The stir tube experiment demonstrated the relative ease with which magnetic stirrers could be added to the system, with beneficial effects on culture growth. With regards to lighting, a shaded system where light was supplied only by an intentional light source (unlike the system used for this project, which was illuminated not just by the growth light, but light in the room and occasionally sunlight, too) would give a greater control over growth conditions. Light could be provided to each individual tube with LED-strips, which would allow for the system to investigate the treatment effect of different light regimes, as well. Finally, a system for temperature control should be implemented, which could take the form of water cooling/heating, making the system a standalone cultivation vessel, not depending on a cultivation cabinet for lighting and temperature.

The improved mini-chemostat array as visualized here is a model created using the Easel Free CNC software by Inventables, and would be an aluminum block into which the ministats could be inserted. The area needed for such a system would be 100mm x 300mm (fig. 38), and could fit the same amount of ministats as the system developed in this project. The aluminum block would not only make the system more compact, but also achieve light control (slots are made which can fit LED-strips, fig 38), and an internal channel running between the two rows of ministat wells could be constructed, through which water could be

pumped, which would give the system an internal temperature control. As the model was made using freeware which only allowed designing in two dimensions, such a channel could not be visualized, but can be achieved by drilling, or by creating the system in blocks, and fixing them together. At the bottom of the ministat wells, there can be a slot for a stopper motor, which could provide magnetic stirring. The system could also be lifted slightly from the ground to allow space for the motherboards required to operate the motors.

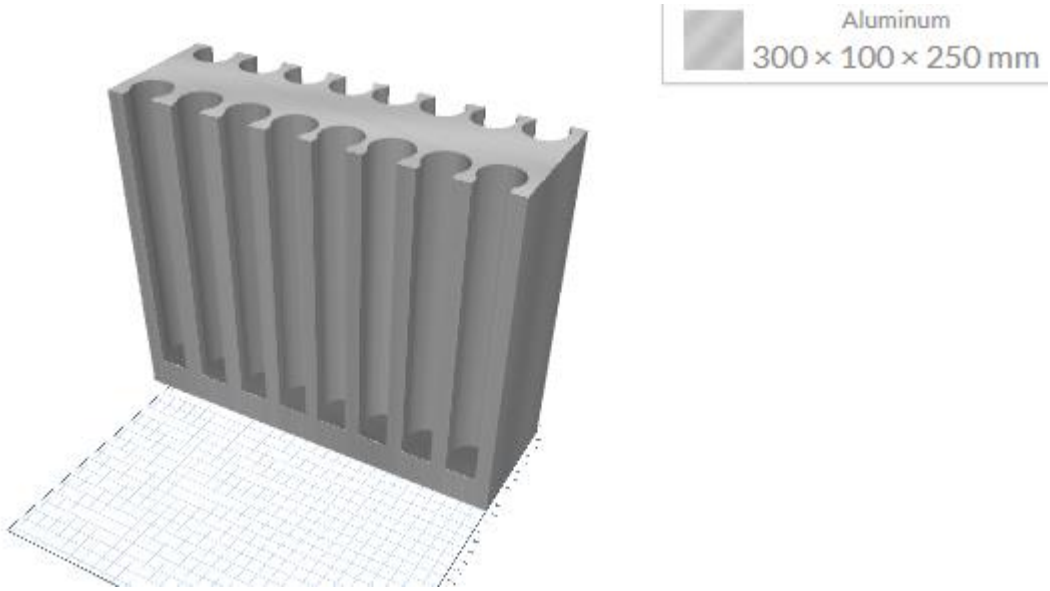

Figure 38 The basic block forming the suggested Mark 2 mini-chemostat array (dimensions W300xL100xD250 mm; created with Easel Free CNC by Inventables).

References

Barkia, I., Saari, N., & Manning, S. R. (2019). Microalgae for High-Value Products Towards Human Health and Nutrition. *Marine Drugs*, *17*(5). https://doi.org/10.3390/MD17050304

Barrick, J. E., Yu, D. S., Yoon, S. H., Jeong, H., Oh, T. K., Schneider, D., … Kim, J. F. (2009). Genome evolution and adaptation in a long-term experiment with Escherichia coli. *Nature*, *461*(7268), 1243–1247. https://doi.org/10.1038/NATURE08480

Bennett, A. F., & Hughes, B. S. (2009). Microbial experimental evolution. *American Journal of Physiology. Regulatory, Integrative and Comparative Physiology*, *297*(1). https://doi.org/10.1152/AJPREGU.90562.2008

Bergenholm, D., Liu, G., Hansson, D., & Nielsen, J. (2019). Construction of mini-chemostats for high-throughput strain characterization. *Biotechnology and Bioengineering*, *116*(5), 1029–1038. https://doi.org/10.1002/BIT.26931

Borowitzka, M. A. (1995). Microalgae as sources of pharmaceuticals and other biologically active compounds. *Journal of Applied Phycology 1995 7:1*, *7*(1), 3–15. https://doi.org/10.1007/BF00003544

Caporgno, M. P., & Mathys, A. (2018). Trends in Microalgae Incorporation Into Innovative Food Products With Potential Health Benefits. *Frontiers in Nutrition*, *5*, 58. https://doi.org/10.3389/FNUT.2018.00058/BIBTEX

Chatterjee, R., & Yuan, L. (2006). Directed evolution of metabolic pathways. *Trends in Biotechnology*, *24*(1), 28–38. https://doi.org/10.1016/J.TIBTECH.2005.11.002

Chew, K. W., Yap, J. Y., Show, P. L., Suan, N. H., Juan, J. C., Ling, T. C., … Chang, J. S. (2017). Microalgae biorefinery: High value products perspectives. *Bioresource Technology*, *229*, 53–62. https://doi.org/10.1016/J.BIORTECH.2017.01.006

Chisti, Y. (2013). Constraints to commercialization of algal fuels. *Journal of Biotechnology*, *167*(3), 201–214. https://doi.org/10.1016/J.JBIOTEC.2013.07.020

Chu, F. F., Shen, X. F., Lam, P. K. S., & Zeng, R. J. (2015). Polyphosphate during the regreening of Chlorella vulgaris under nitrogen deficiency. *International Journal of Molecular Sciences*, *16*(10), 23355–23368. https://doi.org/10.3390/IJMS161023355

Conrad, T. M., Lewis, N. E., & Palsson, B. O. (2011). Microbial laboratory evolution in the era of genome-scale science. *Molecular Systems Biology*, *7*. https://doi.org/10.1038/MSB.2011.42

Cooper, V. S., & Lenski, R. E. (2000). The population genetics of ecological specialization in evolving Escherichia coli populations. *Nature*, *407*(6805), 736–739. https://doi.org/10.1038/35037572

Dallinger WH. The president's address. J R Microsc Soc 10: 185–199, 1887.

Dragosits, M., & Mattanovich, D. (2013). Adaptive laboratory evolution - principles and applications for biotechnology. *Microbial Cell Factories*, *12*(1), 1–17. https://doi.org/10.1186/1475-2859-12-64/TABLES/2

Gonzalez, A., & Bell, G. (2013). Evolutionary rescue and adaptation to abrupt environmental change depends upon the history of stress. *Philosophical Transactions of the Royal Society B: Biological Sciences*, *368*(1610). https://doi.org/10.1098/RSTB.2012.0079

Gresham, D., & Dunham, M. J. (2014). The enduring utility of continuous culturing in experimental evolution. *Genomics*, *104*(6 Pt A), 399–405. https://doi.org/10.1016/J.YGENO.2014.09.015

Japar, A. S., Takriff, M. S., & Mohd Yasin, N. H. (2021). Microalgae acclimatization in industrial wastewater and its effect on growth and primary metabolite composition. *Algal Research*, *53*, 102163. https://doi.org/10.1016/J.ALGAL.2020.102163

Jeong, H., Lee, S. J., & Kim, P. (2016). Procedure for Adaptive Laboratory Evolution of Microorganisms Using a Chemostat. *Journal of Visualized Experiments : JoVE*, *2016*(115). https://doi.org/10.3791/54446

Khan, M. I., Shin, J. H., & Kim, J. D. (2018). The promising future of microalgae: current status, challenges, and optimization of a sustainable and renewable industry for biofuels, feed, and other products. *Microbial Cell Factories 2018 17:1*, *17*(1), 1–21. https://doi.org/10.1186/S12934-018-0879-X

Kim, T. Y., Sohn, S. B., Kim, H. U., & Lee, S. Y. (2008). Strategies for systems-level metabolic engineering. *Biotechnology Journal*, *3*(5), 612–623. https://doi.org/10.1002/BIOT.200700240

Kumari, K., Samantaray, S., Sahoo, D., & Tripathy, B. C. (2021). Nitrogen, phosphorus and high CO2 modulate photosynthesis, biomass and lipid production in the green alga Chlorella vulgaris. *Photosynthesis Research*, *148*(1–2), 17–32. https://doi.org/10.1007/S11120-021-00828-0/FIGURES/8

Lam, M. K., Lee, K. T., & Mohamed, A. R. (2012). Current status and challenges on microalgae-based carbon capture. *International Journal of Greenhouse Gas Control*, *10*, 456–469. https://doi.org/10.1016/J.IJGGC.2012.07.010

LaPanse, A. J., Krishnan, A., & Posewitz, M. C. (2021). Adaptive Laboratory Evolution for algal strain improvement: methodologies and applications. *Algal Research*, *53*, 102122. https://doi.org/10.1016/J.ALGAL.2020.102122

Lee, S. R., & Kim, P. (2020). Current Status and Applications of Adaptive Laboratory Evolution in Industrial Microorganisms. *Journal of Microbiology and Biotechnology*, *30*(6), 793–803. https://doi.org/10.4014/JMB.2003.03072

Lenski, R. E., & Burnham, T. C. (2018). Experimental evolution of bacteria across 60,000 generations, and what it might mean for economics and human decision-making. *Journal of Bioeconomics*, *20*(1), 107–124. https://doi.org/10.1007/S10818-017-9258-7/TABLES/1

Lenski, R. E., Mongold, J. A., Sniegowski, P. D., Travisano, M., Vasi, F., Gerrish, P. J., & Schmidt, T. M. (1998). Evolution of competitive fitness in experimental populations of E. coli: What makes one genotype a better competitor than another? *Antonie van Leeuwenhoek, International Journal of General and Molecular Microbiology*, *73*(1), 35–47. https://doi.org/10.1023/A:1000675521611

Liu, L., Li, Y., Li, S., Hu, N., He, Y., Pong, R., … Law, M. (2012). Comparison of next-generation sequencing systems. *Journal of Biomedicine & Biotechnology*, *2012*. https://doi.org/10.1155/2012/251364

Mandalam, R. K., & Palsson, B. (1998). Elemental balancing of biomass and medium composition enhances growth capacity in high-density Chlorella vulgaris cultures. *Biotechnology and Bioengineering*, *59*(5), 605–611. https://doi.org/10.1002/(sici)1097-0290(19980905)59:5<605::aid-bit11>3.0.co;2-8

Mehariya, S., Goswami, R. K., Karthikeysan, O. P., & Verma, P. (2021). Microalgae for high-value products: A way towards green nutraceutical and pharmaceutical compounds. *Chemosphere*, *280*, 130553. https://doi.org/10.1016/J.CHEMOSPHERE.2021.130553

Monod, J. (2003). The Growth of Bacterial Cultures. *Https://Doi.Org/10.1146/Annurev.Mi.03.100149.002103*, *3*(1), 371–394. https://doi.org/10.1146/ANNUREV.MI.03.100149.002103

Monod, J. (1950). Technique, Theory and Applications of Continuous Culture. *Ann. Inst. Pasteur*, *79*(4), 390–410.

Mukhopadhyay, A., Redding, A. M., Rutherford, B. J., & Keasling, J. D. (2008). Importance of systems biology in engineering microbes for biofuel production. *Current Opinion in Biotechnology*, *19*(3), 228–234. https://doi.org/10.1016/J.COPBIO.2008.05.003

Myers, J., & Clark, L. B. (1944). CULTURE CONDITIONS AND THE DEVELOPMENT OF THE PHOTOSYNTHETIC MECHANISM : II. AN APPARATUS FOR THE CONTINUOUS CULTURE OF CHLORELLA. *The Journal of General Physiology*, *28*(2), 103–112. https://doi.org/10.1085/JGP.28.2.103

NOVICK, A., & SZILARD, L. (1950a). Experiments with the Chemostat on spontaneous mutations of bacteria. *Proceedings of the National Academy of Sciences of the United States of America*, *36*(12), 708–719. https://doi.org/10.1073/PNAS.36.12.708

Novick, A., & Szilard, L. (1950b). Description of the chemostat. *Science (New York, N.Y.)*, *112*(2920), 715–716. https://doi.org/10.1126/SCIENCE.112.2920.715

Portnoy, V. A., Bezdan, D., & Zengler, K. (2011). Adaptive laboratory evolution--harnessing the power of biology for metabolic engineering. *Current Opinion in Biotechnology*, *22*(4), 590–594. https://doi.org/10.1016/J.COPBIO.2011.03.007

Radakovits, R., Jinkerson, R. E., Darzins, A., & Posewitz, M. C. (2010). Genetic Engineering of Algae for Enhanced Biofuel Production. *Eukaryotic Cell*, *9*(4), 486. https://doi.org/10.1128/EC.00364-09

Rao, V. S. H., & Rao Sekhara, P. R. (2004). Global stability in chemostat models involving time delays and wall growth. *Nonlinear Analysis: Real World Applications*, *5*(1), 141–158. https://doi.org/10.1016/S1468-1218(03)00022-1

Safi, C., Zebib, B., Merah, O., Pontalier, P. Y., & Vaca-Garcia, C. (2014). Morphology, composition, production, processing and applications of Chlorella vulgaris: A review. *Renewable and Sustainable Energy Reviews*, *35*, 265–278. https://doi.org/10.1016/J.RSER.2014.04.007

Sandberg, T. E., Salazar, M. J., Weng, L. L., Palsson, B. O., & Feist, A. M. (2019). The emergence of adaptive laboratory evolution as an efficient tool for biological discovery and industrial biotechnology. *Metabolic Engineering*, *56*, 1–16. https://doi.org/10.1016/J.YMBEN.2019.08.004

Sarker, P. K., Kapuscinski, A. R., McKuin, B., Fitzgerald, D. S., Nash, H. M., & Greenwood, C. (2020). Microalgae-blend tilapia feed eliminates fishmeal and fish oil, improves growth, and is cost viable. *Scientific Reports 2020 10:1*, *10*(1), 1–14. https://doi.org/10.1038/s41598-020-75289-x

Sayre, R. (2010). Microalgae: The Potential for Carbon Capture. *BioScience*, *60*(9), 722–727. https://doi.org/10.1525/BIO.2010.60.9.9

Shurin, J. B., Abbott, R. L., Deal, M. S., Kwan, G. T., Litchman, E., Mcbride, R. C., … Smith, V. H. (2013). Industrial-strength ecology: trade-offs and opportunities in algal biofuel production. *Ecology Letters*, *16*(11), 1393–1404. https://doi.org/10.1111/ELE.12176

Skelding, D., Hart, S. F. M., Vidyasagar, T., Pozhitkov, A. E., & Shou, W. (2018). Developing a low-cost milliliter-scale chemostat array for precise control of cellular growth. *Quantitative Biology (Beijing, China)*, *6*(2), 129–141. https://doi.org/10.1007/S40484-018-0143-8

Suzuki, H., Hulatt, C. J., Wijffels, R. H., & Kiron, V. (2019). Growth and LC-PUFA production of the cold-adapted microalga Koliella antarctica in photobioreactors. *Journal of Applied Phycology*, *31*(2), 981–997. https://doi.org/10.1007/S10811-018-1606-Z/FIGURES/5

Takahashi, C. N., Miller, A. W., Ekness, F., Dunham, M. J., & Klavins, E. (2015). A low cost, customizable turbidostat for use in synthetic circuit characterization. *ACS Synthetic Biology*, *4*(1), 32–38. https://doi.org/10.1021/SB500165G/SUPPL_FILE/SB500165G_SI_003.ZIP

Yuan, S. F., & Alper, H. S. (2019). Metabolic engineering of microbial cell factories for production of nutraceuticals. *Microbial Cell Factories*, *18*(1), 1–11. https://doi.org/10.1186/S12934-019-1096-Y/FIGURES/1

Ziv, N., Brandt, N. J., & Gresham, D. (2013). The use of chemostats in microbial systems biology. *Journal of Visualized Experiments : JoVE*, (80). https://doi.org/10.3791/50168

Zimny, T., Sowa, S., Tyczewska, A., & Twardowski, T. (2019). Certain new plant breeding techniques and their marketability in the context of EU GMO legislation – recent developments. *New Biotechnology*, *51*, 49–56. https://doi.org/10.1016/J.NBT.2019.02.003

Appendix A Supplementary tables

First continuous cultivation

Table A-1 The absolute value of optical density at lambda 540 per tube; all tubes grown with Control M8 medium

Hour	Tube 1	Tube 2	Tube 3	Tube 4	Average	SD
0	0.306	0.326	0.323	0.314	0.31725	0.009069
25	0.572	0.509	0.539	0.525	0.53625	0.0268
49	0.65	0.729	0.644	0.571	0.6485	0.064573
97	3.58	5.21	4.22	4.36	4.3425	0.67064
169	14.86	15.5	16.3	12.08	14.685	1.833858
217	20.6	21.32	23.88	29.92	23.93	4.234131
289	24.75	11.85	27.3	20.3	21.05	6.781224
339	28.95	23.95	29.7	20.3	25.725	4.42653
359	27.95	24.5	29.35	20.1	25.475	4.122398

Second continuous cultivation

Table A-2 The absolute value of optical density at lambda 540 per ministat; 3 treatments, M8, N25, P25.

Treatment	Sample	0H	36H	94H	142H	190H	240H	287H	331H
Control	1	0.592	1.864	6.99	15.2	17.8	20.15	21.95	20.5
Control	2	0.595	2.432	7.18	14.65	21.15	22.65	21.75	21.5
Control	3	0.604	1.596	7.16	15.35	18.2	22.05	22.25	22.75
Control	4	0.587	1.38	13.62	15.25	25.55	25.7	35.35	31.65
N25	5	0.604	2.024	11.44	22.7	23.9	25.65	24.3	20.65
N25	6	0.604	1.716	11.4	20.45	18.4	20.55	23.25	21.45
N25	7	0.677	1.64	11.26	22.3	21.4	23.2	20.65	18.3
N25	8	0.609	2.004	11.44	21.95	21.65	21.65	19.3	16
P25	9	0.61	1.544	10.92	20.65	22.9	24.9	24.6	19.65
P25	10	0.605	2.292	11.96	20.4	20.5	22.4	22.95	21.7
P25	11	0.592	1.72	12.86	23.3	24.3	27.2	28.3	27.8
P25	12	0.595	1.668	12.06	22.4	25.4	27.8	30	26.95
Control	13	0.603	1.768	7.2	14.95	19.6	27.85	25.75	23.4
Control	14	0.588	1.644	7.54	15.75	19.05	23.1	23.4	23.7
Control	15	0.612	1.704	7.54	15.6	19.3	22.9	18.75	21.55
Control	16	0.598	1.468	6.99	14.35	16.7	21	20.55	24.1

Growth in terms of weight (Second continuous cultivation)

Table A-3 the weight of dry biomass of algae at inoculation, calculated to g/L.

Sample	Weight before (mg)	Weight after(mg)	Dry mass algae (mg)	Volume(mL)	Biomass (g/L)
1	252.2	256.6	4.4	4	1.1
2	254.5	258.5	4	4	1
3	251.9	253.6	1.7	4	0.425
4	251.3	254.4	3.1	4	0.775
5	251.9	255.7	3.8	4	0.95
6	254.5	257.5	3	4	0.75
7	252.7	256.9	4.2	4	1.05
8	251.6	256.7	5.1	4	1.275
9	250.9	256.2	5.3	4	1.325
10	251.1	256.9	5.8	4	1.45
11	253.6	255.8	2.2	4	0.55
12	253.9	255.9	2	4	0.5
13	251.6	255.9	4.3	4	1.075
14	252.7	256.6	3.9	4	0.975
15	252	257.2	5.2	4	1.3
16	251.9	256.1	4.2	4	1.05

Table A-4 the weight of dry biomass of algae at termination of cultivation, calculated to g/L.

Sample	Weight pre(mg)	Weight post(mg)	Dry weight algae (mg)	Volume(mL)	Biomass (g/L)
1	260.3	278.1	17.8	3	5.933333
2	259.6	276.6	17	3	5.666667
3	259.8	277.9	18.1	3	6.033333
4	260.1	285.1	25	3	8.333333
5	259	275.9	16.9	3	5.633333
6	260.2	276.2	16	3	5.333333
7	259.2	273.4	14.2	3	4.733333
8	261.8	274.4	12.6	3	4.2
9	258.9	274.1	15.2	3	5.066667
10	258.8	274.8	16	3	5.333333
11	259.1	278.4	19.3	3	6.433333
12	259.1	278.2	19.1	3	6.366667
13	257.7	276.1	18.4	3	6.133333
14	258.6	276.8	18.2	3	6.066667
15	259	274.5	15.5	3	5.166667
16	260	273.3	13.3	3	4.433333

Growth in terms of cell count (second continuous cultivation)

Table A-5 the cells per mL culture

Sample	Cell Count	Diameter (µm)	SD (µm)
1 M8	81276	2.83	0.547
2 M8	65 024	3.035	0.561
3 M8	84 055	2.965	0.575
4 M8	106115	2.893	0.506
5 N25	55613	2.889	0.506
6 N25	60 228	2.804	0.467
7 N25	50 785	2.891	0.476
8 N25	43 089	2.891	0.503
9 P25	83 768	2.722	0.525
10 P25	96 828	2.585	0.473
11 P25	107 038	2.553	0.466
12 P25	129 833	2.607	0.487
13 M8	87 359	2.846	0.524
14 M8	89 845	2.808	0.539
15 M8	85 066	3.138	0.568
16 M8	92 406	3.16	0.606

Correlations of Cell count / Optical density / Dry weight

Table A-6 Correlations between cell count, biomass (g/L), and optical density (absorbance at 540nm).

Sample	**Correlation cell count/Dry Weight**		**Correlation OD/Dry weight**		**Correlation OD/cell count**	
1	**Dry weight**	**Cells/mL**	**OD**	**Dry weight**	**OD**	**Cells/mL**
2	5.933333	8.13E+08	20.5	5.933333	20.5	8.13E+08
3	5.666667	6.5E+08	21.5	5.666667	21.5	6.5E+08
4	6.033333	8.41E+08	22.75	6.033333	22.75	8.41E+08
5	8.333333	1.06E+09	31.65	8.333333	31.65	1.06E+09
6	5.633333	5.56E+08	20.65	5.633333	20.65	5.56E+08
7	5.333333	6.02E+08	21.45	5.333333	21.45	6.02E+08
8	4.733333	5.08E+08	18.3	4.733333	18.3	5.08E+08
9	4.2	4.31E+08	16	4.2	16	4.31E+08
10	5.066667	8.38E+08	19.65	5.066667	19.65	8.38E+08
11	5.333333	9.68E+08	21.7	5.333333	21.7	9.68E+08
12	6.433333	1.07E+09	27.8	6.433333	27.8	1.07E+09
13	6.366667	1.3E+09	26.95	6.366667	26.95	1.3E+09
14	6.133333	8.74E+08	23.4	6.133333	23.4	8.74E+08
15	6.066667	8.98E+08	23.7	6.066667	23.7	8.98E+08
16	5.166667	8.51E+08	21.55	5.166667	21.55	8.51E+08
	4.433333	9.24E+08	24.1	4.433333	24.1	9.24E+08
	Correlation coefficient		**Correlation** coefficient:		**Correlation** coefficient:	
	0.590395		0.839836		0.807098	

Third continuous cultivation

Table A-7 The absolute value of optical density at lambda 540 per ministat; 3 treatments, M8, N25, P25

Treatment	Sample	0	24	48	72	96	120	144	168
Control	1	0.042	0.071	0.106	0.286	0.882	2.72	4.7	5.2
Control	2	0.037	0.079	0.171	0.423	2.75	4.83	5.94	6.16
Control	3	0.037	0.073	0.096	0.236	1.41	3.47	5.14	5.24
Control	4	0.034	0.085	0.197	0.614	3.6	5.74	9.12	13.4
N-	5	0.038	0.079	0.106	0.315	0.96	3.99	10.82	9.48
N-	6	0.037	0.082	0.083	0.241	1.08	4.22	8.8	9
N-	7	0.035	0.074	0.082	0.282	1.14	3.57	8.24	14.64
N-	8	0.033	0.087	0.101	0.231	0.81	2.52	4.76	6.4
P-	9	0.025	0.061	0.103	0.243	0.79	2.23	4.56	5.6
P-	10	0.024	0.059	0.05	0.105	0.56	2.12	4.24	5.64
P-	11	0.028	0.069	0.103	0.309	1.32	3.93	9.8	9.56
P-	12	0.026	0.062	0.103	0.261	1.09	3.1	5.44	6.36
Control	13	0.038	0.121	0.306	1.356	4.52	12.98	8.96	8.16
Control	14	0.035	0.79	0.131	0.244	1.05	3.26	5.48	6.04
Control	15	0.041	0.119	0.301	1.434	4.66	9.78	10.14	9.84
Control	16	0.031	0.139	0.162	0.354	1.18	2.73	5.34	6.84

Growth in terms of weight (Third continuous cultivation)

Table A-8 the weight of dry biomass of algae at inoculation, calculated to g/L.

Sample	Weight pre (mg)	Weight post (mg)	Dry weight (mg)	Volume (mL)	Biomass (g/L)
1	259.7	265.5	5.8	5	1.16
2	257.8	263.1	5.3	5	1.06
3	257.4	262	4.6	5	0.92
4	258.4	263.2	4.8	5	0.96
5	256.3	258.7	2.4	5	0.48
6	254.3	256.3	2	5	0.4
7	256	258.3	2.3	5	0.46
8	254	256	2	5	0.4
9	256.3	260.4	4.1	5	0.82
10	256	260.2	4.2	5	0.84
11	257	260.9	3.9	5	0.78
12	255.1	259	3.9	5	0.78
13	256.3	261.6	5.3	5	1.06
14	257.5	262.2	4.7	5	0.94
15	251.3	255.7	4.4	5	0.88
16	254.4	258.9	4.5	5	0.9

Table A-9 The weight of dry biomass of algae at termination of cultivation, calculated to g/L

Sample	Weight pre (mg)	Weight post(mg)	Dryweight (mg)	Volume(mL)	Biomass (g/L)
1	254.6	260.2	5.6	3	1.866667
2	255.5	262	6.5	3	2.166667
3	257.2	261.9	4.7	3	1.566667
4	256.9	271	14.1	3	4.7
5	255.9	268.4	12.5	3	4.166667
6	254.7	259.2	4.5	3	1.5
7	250.5	255.3	4.8	3	1.6
8	248.5	252.8	4.3	3	1.433333
9	251.1	257.5	6.4	3	2.133333
10	254.3	264.9	10.6	3	3.533333
11	256.9	268.5	11.6	3	3.866667
12	254.9	264.5	9.6	3	3.2
13	255.4	261	5.6	3	1.866667
14	253.8	259.8	6	3	2
15	256.3	261.3	5	3	1.666667
16	254.6	261.8	7.2	3	2.4

Fourth continuous cultivation

Table A-10 The absolute value of optical density at lambda 540 per ministat; 3 treatments, M8, N25, P25.

Treatment	Sample	0H	16H	38H	62H	86H	110H	134H	158H	182H	206H
C	1	0.173	0.341	0.713	1.548	1.488	1.605	1.39	1.47	1.428	1.272
C	2	0.176	0.289	0.843	2.24	2.604	2.905	2.665	3.255	3.354	3.918
C	3	0.19	0.379	0.803	1.588	1.76	1.795	1.41	1.675	1.578	2.07
C	4	0.177	0.271	0.705	1.812	2.204	2.51	3.295	5.528	5.49	3.408
P	5	0.195	0.313	1.121	1.988	2.02	2.195	1.73	1.95	2.208	1.908
P	6	0.196	0.21	0.467	1.14	1.756	2.095	1.8	2.015	1.83	1.812
P	7	0.203	0.236	0.706	1.592	2.22	2.375	2.08	2.575	2.598	2.628
P	8	0.182	0.209	0.578	1.636	2.312	2.575	2.38	2.765	2.796	2.802
N	9	0.156	0.278	0.804	1.864	1.612	2.95	1.895	3.27	2.292	1.434
N	10	0.155	0.25	0.719	1.448	0.876	2.545	0.945	2.565	1.83	1.698
N	11	0.151	0.272	0.673	1.048	0.992	1.02	0.88	0.9	0.996	1.392
N	12	0.137	0.291	0.886	0.916	1.288	0.975	0.715	0.885	1.278	1.2
C	13	0.186	0.301	0.833	1.972	2.224	2.8	1.91	1.64	2.064	2.208
C	14	0.175	0.298	0.745	1.548	1.888	2.18	1.785	2.195	2.262	2.334
C	15	0.18	0.319	0.71	1.4	1.756	2.05	1.27	1.34	1.23	1.146
C	16	0.181	0.279	0.73	1.484	1.6	1.905	1.5	1.79	1.968	2.07
Treatment	**Sample**	**230H**	**254H**	**278H**	**302H**	**328H**	**352H**	**376H**	**400H**	**424H**	**448H**

C	1	1.482	1.644	1.494	1.65	1.65	1.806	1.86	1.962	1.95	1.776
C	2	2.952	3.168	3.096	2.958	2.916	2.922	3.114	2.67	2.448	2.244
C	3	1.572	2.034	1.914	1.47	1.38	1.464	1.704	1.968	1.452	1.362
C	4	2.394	3.63	3.114	2.514	1.524	2.034	1.938	1.986	2.13	2.064
P	5	1.848	2.316	2.4	2.52	0.996	2.52	2.562	2.304	2.562	2.58
P	6	1.482	2.292	2.208	2.262	2.118	2.358	2.352	2.73	2.466	2.358
P	7	2.166	3.114	3.216	3.252	3.51	5.208	4.104	2.238	3.012	2.772
P	8	2.736	3.57	3.45	3.666	3.42	3.678	4.59	3.912	2.778	2.076
N	9	0.63	4.344	2.496	4.044	3.18	2.076	4.188	1.758	1.758	1.35
N	10	0.144	3.528	0.75	2.256	0.984	0.714	2.418	0.984	2.154	2.214
N	11	0.798	1.368	2.004	1.746	0.426	2.004	1.356	0.954	2.352	1.65
N	12	1.086	1.368	1.332	1.152	0.828	0.822	0.798	0.87	0.7134	1.206
C	13	2.682	3.402	3.54	5.046	3.558	3.408	3.018	5.106	3.39	3.072
C	14	2.4	3.438	4.104	3.066	2.46	2.31	2.232	2.142	2.136	2.154
C	15	1.272	1.998	1.548	1.2	1.05	0.828	0.786	0.714	1.338	1.83
C	16	1.71	2.112	2.178	2.118	2.004	2.556	2.124	3.534	2.82	2.52
Treatment	**Sample**	**472H**	**496H**	**520H**	**544H**	**568H**	**592H**	**616H**	**640H**	**664H**	**688H**
C	1	2.376	1.848	2.73	2.412	2.058	2.286	3.498	3.354	2.742	4.578
C	2	2.094	2.13	2.148	2.1	1.878	1.86	1.83	2.172	1.8	2.322
C	3	1.47	1.764	2.232	2.136	2.07	3.372	4.626	4.212	3.558	3.15
C	4	1.812	1.974	2.01	1.926	1.758	1.71	1.386	1.296	1.338	1.512
P	5	3.018	2.73	2.664	3.036	2.694	1.542	1.62	2.112	0.486	1.446
P	6	2.226	2.064	2.484	2.328	2.058	1.26	0.798	0.834	0.264	0.474
P	7	2.676	2.322	2.484	2.658	2.526	1.746	0.978	0.606	0.768	0.69
P	8	1.692	2.43	3.246	2.322	1.716	1.068	0.912	1.002	1.218	0.948
N	9	3.858	2.394	1.038	1.626	1.254	1.326	2.016	1.158	1.044	1.638
N	10	1.05	1.614	1.62	1.482	1.71	2.142	1.314	0.72	0.09	0.762
N	11	0.984	1.308	2.388	1.92	0.918	1.224	0.9	1.26	0.72	1.518
N	12	1.17	2.184	1.524	1.152	0.918	0.9	0.93	1.224	0.396	1.86
C	13	2.964	2.694	2.514	2.778	2.454	2.568	2.544	2.334	2.052	2.412
C	14	2.07	2.178	1.878	1.722	1.272	1.386	1.56	1.962	2.136	2.136
C	15	2.334	2.322	2.238	2.052	2.004	2.022	1.446	1.554	1.92	2.466
C	16	2.292	2.532	3.372	3.18	2.964	3.348	4.026	3.906	3.186	3.312

Fifth continuous cultivation

Table A-11 The absolute value of optical density at lambda 540 per ministat; 5 treatments, M8, N5, N10, P5, and P10.

Treatment	**Sample**	**0H**	**18H**	**34H**	**61H**	**92H**	**114H**	**138H**	**210H**	**236H**	**285H**	**331H**	**380H**	**39**
Control	1	0.069	0.11	0.17	0.284	1.595	2.82	2.6	3.58	2.64	2.64	2.85	1.51	1
N5	2	0.087	0.051	0.092	0.148	0.4	0.83	0.9	1.1	2.24	1.29	1.119	0.56	0
N10	3	0.036	0.057	0.096	0.152	0.61	1.38	1.35	2.01	2.17	1.66	1.34	0.51	0
P5	4	0.06	0.108	0.181	0.345	1.065	0.63	2.53	0.93	2.44	2.59	3.3	2.91	3
P10	5	0.061	0.098	0.151	0.321	0.65	0.35	0.61	1.34	0.49	1.11	1.81	2.12	2

Control	6	0.137	0.205	0.291	0.577	1.43	1.88	2.72	2.9	3.06	2.68	2.64	2.07	1
N5	7	0.067	0.172	0.162	0.226	0.595	0.79	1	1.32	1.68	1.37	1.255	0.45	0
N10	8	0.064	0.072	0.124	0.294	1.115	2.07	2.27	2.75	2.92	2.47	2.34	0.96	1
P5	9	0.046	0.08	0.114	0.25	0.935	0.59	1.27	1.03	1.96	2.1	3.21	2.09	2
P10	10	0.068	0.088	0.138	0.321	1.26	1.11	1.88	1.87	2.94	4.1	5.29	3.13	3
Control	11	0.063	0.192	0.198	0.266	0.6	1.07	1.65	1.7	2.2	1.71	1.23	0.65	1
N5	12	0.044	0.106	0.086	0.148	0.405	0.58	0.58	0.46	0.58	0.42	0.44	0.76	0
N10	13	0.044	0.117	0.097	0.398	1.97	2.5	3.43	2.81	3.28	3.38	3.21	2.59	2
P5	14	0.056	0.103	0.124	0.261	0.7	0.44	1.63	4.09	1.74	0.82	4.06	3.98	3
P10	15	0.062	0.093	0.094	0.179	0.565	0.525	0.87	0.82	1.45	0.27	0.88	0.97	1
Control	16	0.085	0.154	0.176	0.252	0.94	2.31	2.3	2.65	2.87	2.51	2.51	2.38	1

Growth in terms of weight (fifth continuous cultivation)

Table A-12 the weight of dry biomass of algae at inoculation, calculated to g/L.

Sample	Weight pre (mg)	Weight post (mg)	Dry mass algae(mg)	Volume(mL)	Biomass (g/L)
1	250	252.3	2.3	4	0.575
2	250	252.6	2.6	5	0.52
3	251.1	253.2	2.1	4	0.525
4	252.5	256	3.5	4	0.875
5	251.2	255.1	3.9	4	0.975
6	254	259	5	4	1.25
7	255.8	257.9	2.1	4	0.525
8	248.7	249.9	1.2	4	0.3
9	255.5	256.5	1	4	0.25
10	254.6	257.6	3	4	0.75
11	254.6	258.8	4.2	4	1.05
12	255	257.1	2.1	4	0.525
13	257.7	260	2.3	4	0.575
14	253.4	257.7	4.3	4	1.075
15	251.7	255.4	3.7	4	0.925
16	251.2	255.5	4.3	4	1.075

Table A-13 The weight of dry biomass of algae at termination of cultivation, calculated to g/L

Sample	Weight pre (mg)	Weight post (mg)	Dry mass algae(mg)	Volume(mL)	Biomass (g/L)
1	252.1	259.5	7.4	3	2.466667
2	250.2	253.5	3.3	3	1.1
3	250.9	253.7	2.8	3	0.933333
4	257.8	268.2	10.4	3	3.466667
5	255.4	264.6	9.2	3	3.066667
6	260.3	269.5	9.2	3	3.066667

7	256.5	259.5	3	3	1
8	253.7	258	4.3	3	1.433333
9	254.2	262.4	8.2	3	2.733333
10	254	263.4	9.4	3	3.133333
11	252.3	260.5	8.2	3	2.733333
12	258.9	262.7	3.8	3	1.266667
13	255.4	261.1	5.7	3	1.9
14	259.3	272	12.7	3	4.233333
15	258.1	261.7	3.6	3	1.2
16	257.9	262.4	4.5	3	1.5

Sixth continuous cultivation

Table A-14 The absolute value of optical density at lambda 540 per ministat; 5 treatments, M8, N5, N10, P5, and P10.

Treatment	Sample	0	64	85	117	159	231	327
Control	1	0.075	0.486	0.956	1.376	1.86	1.91	2.18
N5	2	0.056	0.232	0.492	1.12	1.9	1.9	1.18
N10	3	0.063	0.269	0.558	1.388	1.75	2.18	2.2
P5	4	0.073	0.662	0.984	1.062	0.99	1.89	2.12
P10	5	0.061	0.539	0.423	0.728	0.91	2.37	1.84
Control	6	0.095	0.773	1.3	1.436	1.49	1.55	1.78
N5	7	0.078	0.423	1.03	1.658	2	1.54	1.55
N10	8	0.056	0.431	0.952	1.396	1.71	1.83	2.11
P5	9	0.066	0.403	0.746	1.026	0.83	1.69	1.63
P10	10	0.045	0.683	0.897	1.332	0.91	2.31	3.28
Control	11	0.054	0.214	0.41	0.976	1.18	1.25	1.47
N5	12	0.09	0.359	0.852	1.294	1.67	1.9	2.42
N10	13	0.081	0.471	0.746	0.816	0.7	1.91	1.82
P5	14	0.059	0.233	0.544	0.624	0.41	1.58	1.19
P10	15	0.08	0.318	0.7	1.342	1.87	2.54	2.97
Control	16	0.092	0.548	1.136	1.714	2.14	2.42	2.58

Growth in terms of weight (sixth continuous cultivation)

Table A-15 The weight of dry biomass of algae at inoculation, calculated to g/L

Sample	Weight pre (mg)	Weight post (mg)	Dry mass algae(mg)	Volume(mL)	Biomass (g/L)
1	257.1	263.5	6.4	4	1.6
2	258.6	262.4	3.8	4	0.95
3	260.2	263.5	3.3	4	0.825
4	258.6	263.2	4.6	4	1.15
5	255.7	263.7	8	4	2
6	253.4	261.8	8.4	4	2.1
7	257.4	257.9	0.5	4	0.125

8	257.4	260.7	3.3	4	0.825
9	257.4	262.2	4.8	4	1.2
10	256.7	262	5.3	4	1.325
11	257.2	260.9	3.7	4	0.925
12	258.1	261.2	3.1	4	0.775
13	257	261.5	4.5	4	1.125
14	253.1	257.9	4.8	4	1.2
15	253.7	260	6.3	4	1.575
16	258.6	265.3	6.7	4	1.675

Table A-16 The weight of dry biomass of algae at termination of cultivation, calculated to g/L

Sample	Weight pre (mg)	Weight post (mg)	Dry mass algae(mg)	Volume(mL)	Biomass (g/L)
1	256.1	263	6.9	3	2.3
2	255.6	258	2.4	3	0.8
3	255.2	258.4	3.2	3	1.066667
4	252	258.9	6.9	3	2.3
5	250.8	256.7	5.9	3	1.966667
6	251.6	258.1	6.5	3	2.166667
7	253.9	256.8	2.9	3	0.966667
8	253.1	256.4	3.3	3	1.1
9	253.1	257.5	4.4	3	1.466667
10	251.5	257.4	5.9	3	1.966667
11	257.1	259.3	2.2	3	0.733333
12	250.7	254	3.3	3	1.1
13	251.1	255.6	4.5	3	1.5
14	253.1	261.9	8.8	3	2.933333
15	252	258	6	3	2
16	258.1	263.8	5.7	3	1.9

Appendix B – Supplementary figures

Supplement for 3.1 – Batch growth

```
  sample        k       n0          r    t_mid    t_gen    auc_l    auc_e
1  Tube1 51.77087 1.292251 0.01657951 221.0659 41.80746 6349.420 6371.648
2  Tube2 55.86306 1.335372 0.01607937 230.6993 43.10786 6432.205 6430.936
3  Tube3 54.61871 1.424916 0.01529513 236.6655 45.31817 6082.747 6072.992
4  Tube4 67.80869 1.329185 0.01525801 256.4114 45.42841 6516.565 6578.640
5  Tube5 37.84166 1.041997 0.01632096 218.3910 42.46976 4736.167 4708.332
      sigma note
1 1.2637891
2 1.7787578
3 1.2815731
4 1.4755538
5 0.9567114

Quick summary of variables:
N0: Population at beginning of run
K: Carrying capacity (max population size)
r: Intrinsic growth rate
t: Time (hours); Mid: Halfway to stationary; Gen: Per generation

Max population size (k): 37 to 67
Maximum intrinsic growth rate (r): 0.015 - 0.016
```

Figure B.1 GrowthcurveR-output showing growth variables; note intrinsic growth rate provided per hour

Supplement for 3.3 - Second continuous cultivation

```
Call:
aov(formula = OD ~ Treatment, data = Cont2)

Residuals:
    Min      1Q  Median      3Q     Max
-4.3750 -2.1891 -0.5219  1.7500  8.0063

Coefficients:
                  Estimate Std. Error t value Pr(>|t|)
(Intercept)        23.6437     1.1992  19.716 4.55e-11 ***
TreatmentReduced_N -4.5437     2.0771  -2.188   0.0476 *
TreatmentReduced_P  0.3813     2.0771   0.184   0.8572
---
Signif. codes:  0 ‘***’ 0.001 ‘**’ 0.01 ‘*’ 0.05 ‘.’ 0.1 ‘ ’ 1

Residual standard error: 3.392 on 13 degrees of freedom
Multiple R-squared:  0.3057,    Adjusted R-squared:  0.1988
F-statistic: 2.861 on 2 and 13 DF,  p-value: 0.09338
```

Figure B-2 The R-output ANOVA of optical density

```
Levene's Test for Homogeneity of Variance (center = median)
      Df F value Pr(>F)
group  2  0.5834  0.572
      13

        Shapiro-Wilk normality test

data:  residuals(aov2)
W = 0.9341, p-value = 0.2829

[1] 2.605365
```

Figure B-3 The R-output for the ANOVA assumption tests ¨

```
Call:
aov(formula = Increase ~ Treatment, data = Set2)

Residuals:
     Min       1Q   Median       3Q      Max
-1.61645 -0.97845 -0.05736  0.64138  2.54701

Coefficients:
            Estimate Std. Error t value Pr(>|t|)
(Intercept)   5.0121     0.4073  12.306 1.54e-08 ***
TreatmentN   -1.0478     0.7054  -1.485    0.161
TreatmentP   -0.1730     0.7054  -0.245    0.810
---
Signif. codes:  0 ‘***’ 0.001 ‘**’ 0.01 ‘*’ 0.05 ‘.’ 0.1 ‘ ’ 1

Residual standard error: 1.152 on 13 degrees of freedom
Multiple R-squared:  0.149,     Adjusted R-squared:  0.0181
F-statistic: 1.138 on 2 and 13 DF,  p-value: 0.3503
```

Figure B-4 R-output for ANOVA of dry weights of different treatments

```
Levene's Test for Homogeneity of Variance (center = median)
      Df F value Pr(>F)
group  2  0.2958 0.7488
      13

        Shapiro-Wilk normality test

data:  residuals(Set2AOV)
W = 0.95107, p-value = 0.5067

[1] 2.298703
```

Figure B-5 R-output for ANOVA assumptions of dry weights

```
Call:
aov(formula = OD ~ Treatment, data = Cont3)

Residuals:
   Min     1Q Median     3Q    Max
-2.119 -1.663 -1.369  0.300 10.531

Coefficients:
                  Estimate Std. Error t value Pr(>|t|)
(Intercept)         7.5188     1.2641   5.948 4.84e-05 ***
TreatmentReduced_N -0.6062     2.1895  -0.277    0.786
TreatmentReduced_P -0.8187     2.1895  -0.374    0.714
---
Signif. codes:  0 ‘***’ 0.001 ‘**’ 0.01 ‘*’ 0.05 ‘.’ 0.1 ‘ ’ 1

Residual standard error: 3.575 on 13 degrees of freedom
Multiple R-squared:  0.0126,    Adjusted R-squared:  -0.1393
F-statistic: 0.08295 on 2 and 13 DF,  p-value: 0.9209
```

Figure B-6 R-output for ANOVA of different treatments

```
Levene's Test for Homogeneity of Variance (center = median)
      Df F value Pr(>F)
group  2  0.2054 0.8169
      13

        Shapiro-Wilk normality test

data:  residuals(aov3)
W = 0.61998, p-value = 2.514e-05

[1] 25.78565
```

Figure B-7 R-output for ANOVA assumptions

```
> outlierTest(aov3)
  rstudent unadjusted p-value Bonferroni p
4 6.210057         4.5176e-05   0.00072281
```

Figure B-8 Outlier test

```
> outlierTest(aov3_1)
  rstudent unadjusted p-value Bonferroni p
8 10.52893         4.4068e-07   6.6102e-06
```

Figure B-9 Outlier test 2

```
Call:
aov(formula = OD ~ Treatment, data = Cont3_2)

Residuals:
     Min       1Q   Median       3Q      Max
-1.25000 -0.12857  0.05119  0.24643  0.88571

Coefficients:
                  Estimate Std. Error t value Pr(>|t|)
(Intercept)         6.0143     0.2150  27.970 1.43e-11 ***
TreatmentReduced_N -0.8310     0.3926  -2.117   0.0579 .
TreatmentReduced_P  0.6857     0.3566   1.923   0.0807 .
---
Signif. codes:  0 ‘***’ 0.001 ‘**’ 0.01 ‘*’ 0.05 ‘.’ 0.1 ‘ ’ 1

Residual standard error: 0.5689 on 11 degrees of freedom
Multiple R-squared:  0.5258,    Adjusted R-squared:  0.4396
F-statistic: 6.099 on 2 and 11 DF,  p-value: 0.01651
```

Figure B-10 ANOVA of trimmed data

```
Levene's Test for Homogeneity of Variance (center = median)
      Df F value Pr(>F)
group  2  0.7728 0.4852
      11

        Shapiro-Wilk normality test

data:  residuals(aov3_2)
W = 0.95022, p-value = 0.5641

[1] 53.25
```

Figure B-11 ANOVA assumptions

```
> outlierTest(aov3_2)
No Studentized residuals with Bonferroni p < 0.05
```

Figure B-12 New outlier test

```
Anova Table (Type III tests)

Response: OD
             Sum Sq Df  F value    Pr(>F)
(Intercept) 253.201  1 782.3116 1.428e-11 ***
Treatment     3.948  2   6.0987   0.01651 *
Residuals     3.560 11
---
Signif. codes:  0 ‘***’ 0.001 ‘**’ 0.01 ‘*’ 0.05 ‘.’ 0.1 ‘ ’ 1
```

Figure B-13 New ANOVA

```
Call:
aov(formula = Increase ~ Treatment, data = Set3)

Residuals:
    Min      1Q  Median      3Q     Max
-1.0650 -0.6100 -0.3608  0.2331  2.4458

Coefficients:
            Estimate Std. Error t value Pr(>|t|)
(Intercept)   1.2942     0.3691   3.506  0.00387 **
TreatmentN    0.4458     0.6393   0.697  0.49787
TreatmentP    1.0842     0.6393   1.696  0.11372
---
Signif. codes:  0 ‘***’ 0.001 ‘**’ 0.01 ‘*’ 0.05 ‘.’ 0.1 ‘ ’ 1

Residual standard error: 1.044 on 13 degrees of freedom
Multiple R-squared:  0.1822,    Adjusted R-squared:  0.05633
F-statistic: 1.448 on 2 and 13 DF,  p-value: 0.2706
```

Figure B-14 ANOVA of dry weights

```
Levene's Test for Homogeneity of Variance (center = median)
      Df F value Pr(>F)
group  2  0.0322 0.9684
      13

        Shapiro-Wilk normality test

data:  residuals(Set3AOV)
W = 0.80594, p-value = 0.003269

[1] 2.912329
```

Figure B-15 ANOVA assumptions for dry weights

```
No Studentized residuals with Bonferroni p < 0.05
Largest |rstudent|:
```

Figure B-16 Outlier results for dry weights

```
Call:
aov(formula = Increase ~ Treatment, data = Set3OR)

Residuals:
     Min       1Q   Median       3Q      Max
-1.06500 -0.15310  0.02528  0.15024  0.70833

Coefficients:
            Estimate Std. Error t value Pr(>|t|)
(Intercept)   0.9448     0.1721   5.490 0.000189 ***
TreatmentN    0.1463     0.3142   0.466 0.650433
TreatmentP    1.4336     0.2854   5.024 0.000388 ***
---
Signif. codes:  0 ‘***’ 0.001 ‘**’ 0.01 ‘*’ 0.05 ‘.’ 0.1 ‘ ’ 1

Residual standard error: 0.4553 on 11 degrees of freedom
Multiple R-squared:  0.7093,    Adjusted R-squared:  0.6564
F-statistic: 13.42 on 2 and 11 DF,  p-value: 0.00112
```

Figure B-17 ANOVA for trimmed data (samples 4 & 5 removed)

```
Levene's Test for Homogeneity of Variance (center = median)
      Df F value Pr(>F)
group  2  1.9804 0.1842
      11

        Shapiro-Wilk normality test

data:  residuals(Set3ORAOV)
W = 0.91941, p-value = 0.2156

[1] 199.3916
```

Figure B-18 ANOVA-assumptions for trimmed data (samples 4 & 5 removed)

```
Call:
aov(formula = OD ~ Treatment, data = Cont4)

Residuals:
    Min      1Q  Median      3Q     Max
-1.2240 -0.4144 -0.0705  0.4144  1.8420

Coefficients:
                  Estimate Std. Error t value Pr(>|t|)
(Intercept)         2.7360     0.2651  10.320 1.25e-07 ***
TreatmentReduced_N -1.2915     0.4592  -2.812  0.01468 *
TreatmentReduced_P -1.8465     0.4592  -4.021  0.00145 **
---
Signif. codes:  0 ‘***’ 0.001 ‘**’ 0.01 ‘*’ 0.05 ‘.’ 0.1 ‘ ’ 1

Residual standard error: 0.7499 on 13 degrees of freedom
Multiple R-squared:  0.5887,    Adjusted R-squared:  0.5254
F-statistic: 9.303 on 2 and 13 DF,  p-value: 0.003105
```

Figure B-19 ANOVA of treatments

```
Levene's Test for Homogeneity of Variance (center = median)
      Df F value Pr(>F)
group  2  0.7137  0.508
      13

        Shapiro-Wilk normality test

data:  residuals(aov4)
W = 0.9348, p-value = 0.2901

[1] 4.977256
```

Figure B-20 ANOVA assumptions

```
Call:
aov(formula = OD ~ Treatment, data = Cont5)

Residuals:
    Min      1Q  Median      3Q     Max
-1.0367 -0.3269  0.0800  0.3231  1.0833

Coefficients:
             Estimate Std. Error t value Pr(>|t|)
(Intercept)    1.5075     0.3579   4.212  0.00146 **
TreatmentN10  -0.1408     0.5467  -0.258  0.80147
TreatmentN5   -0.7975     0.5467  -1.459  0.17260
TreatmentP10   0.7692     0.5467   1.407  0.18708
TreatmentP5    1.6292     0.5467   2.980  0.01252 *
---
Signif. codes:  0 ‘***’ 0.001 ‘**’ 0.01 ‘*’ 0.05 ‘.’ 0.1 ‘ ’ 1

Residual standard error: 0.7158 on 11 degrees of freedom
Multiple R-squared:  0.6508,    Adjusted R-squared:  0.5239
F-statistic: 5.126 on 4 and 11 DF,  p-value: 0.01404
```

Figure B-21 ANOVA of treatments

```
Levene's Test for Homogeneity of Variance (center = median)
      Df F value Pr(>F)
group  4  0.6796 0.6203
      11

        Shapiro-Wilk normality test

data:  residuals(aov5)
W = 0.9686, p-value = 0.8155

[1] 48.4915
```

Figure B-22 Assumptions ANOVA

```
Anova Table (Type III tests)

Response: OD
             Sum Sq Df F value   Pr(>F)
(Intercept)  9.0902  1 17.7409 0.001456 **
Treatment   10.5059  4  5.1259 0.014044 *
Residuals    5.6363 11
---
Signif. codes:  0 ‘***’ 0.001 ‘**’ 0.01 ‘*’ 0.05 ‘.’ 0.1 ‘ ’ 1
```

Figure B-23 Type III ANOVA of treatments

```
> outlierTest(aov5)
No Studentized residuals with Bonferroni p < 0.05
```

Figure B-24 Outlier test

```
Call:
aov(formula = Increase ~ Treatment, data = Set5)

Residuals:
    Min      1Q  Median      3Q     Max
-1.3083 -0.1799  0.1603  0.3806  0.8000

Coefficients:
             Estimate Std. Error t value Pr(>|t|)
(Intercept)    1.4542     0.3307   4.398  0.00107 **
TreatmentN10  -0.4986     0.5051  -0.987  0.34479
TreatmentN5   -0.8553     0.5051  -1.693  0.11850
TreatmentP10   0.1292     0.5051   0.256  0.80289
TreatmentP5    1.2903     0.5051   2.554  0.02678 *
---
Signif. codes:  0 ‘***’ 0.001 ‘**’ 0.01 ‘*’ 0.05 ‘.’ 0.1 ‘ ’ 1

Residual standard error: 0.6613 on 11 degrees of freedom
Multiple R-squared:  0.6239,    Adjusted R-squared:  0.4872
F-statistic: 4.563 on 4 and 11 DF,  p-value: 0.02044
```

Figure B-25 ANOVA of dry weights

```
Levene's Test for Homogeneity of Variance (center = median)
      Df F value Pr(>F)
group  4  0.4998 0.7368
      11

        Shapiro-Wilk normality test

data:  residuals(Set5AOV)
W = 0.90878, p-value = 0.1112

[1] 72.32157
```

Figure B-26 ANOVA-assumptions for dry weights

Supplement for 3.7 – Sixth continuous cultivation

```
Call:
aov(formula = OD ~ Treatment, data = Cont6)

Residuals:
    Min      1Q  Median      3Q     Max
-0.8567 -0.2817  0.0250  0.3233  0.7033

Coefficients:
                      Estimate Std. Error t value Pr(>|t|)
(Intercept)            2.00250    0.26838   7.462 1.26e-05 ***
TreatmentReduced_N10   0.04083    0.40995   0.100    0.922
TreatmentReduced_N5   -0.28583    0.40995  -0.697    0.500
TreatmentReduced_P10   0.69417    0.40995   1.693    0.118
```

```
Call:
aov(formula = Increase ~ Treatment, data = Set6)

Residuals:
     Min       1Q   Median       3Q      Max
-0.78333 -0.19444  0.00556  0.14931  0.68333

Coefficients:
             Estimate Std. Error t value Pr(>|t|)
(Intercept)   0.20000    0.22621   0.884   0.3955
TreatmentN10  0.09722    0.34554   0.281   0.7837
TreatmentN5   0.13889    0.34554   0.402   0.6954
TreatmentP10  0.14444    0.34554   0.418   0.6840
TreatmentP5   0.85000    0.34554   2.460   0.0317 *
---
Signif. codes:  0 ‘***’ 0.001 ‘**’ 0.01 ‘*’ 0.05 ‘.’ 0.1 ‘ ’ 1

Residual standard error: 0.4524 on 11 degrees of freedom
Multiple R-squared:  0.3941,    Adjusted R-squared:  0.1738
F-statistic: 1.789 on 4 and 11 DF,  p-value: 0.2013
```

Figure B-28 ANOVA of dry weights

```
Levene's Test for Homogeneity of Variance (center = median)
      Df F value Pr(>F)
group  4  1.0311 0.4338
      11

        Shapiro-Wilk normality test

data:  residuals(Set6AOV)
W = 0.96958, p-value = 0.8317

[1] 113.25
```

Figure B-29 ANOVA assumptions for dry weights

Supplement for 3.8 Effect of flowrate on absorbance

```
Call:
aov(formula = OD ~ Flowrate, data = od_flow)

Residuals:
    Min      1Q  Median      3Q     Max
-5.6151 -0.6312  0.4103  1.1943 11.0190

Coefficients:
            Estimate Std. Error t value Pr(>|t|)
(Intercept)  26.0511     0.8755   29.75   <2e-16 ***
Flowrate    -34.9681     1.4801  -23.62   <2e-16 ***
---
Signif. codes:  0 ‘***’ 0.001 ‘**’ 0.01 ‘*’ 0.05 ‘.’ 0.1 ‘ ’ 1

Residual standard error: 2.921 on 76 degrees of freedom
Multiple R-squared:  0.8802,    Adjusted R-squared:  0.8786
F-statistic: 558.1 on 1 and 76 DF,  p-value: < 2.2e-16
```

Fixure B-30 ANOVA of flowrates

```
Levene's Test for Homogeneity of Variance (center = median)
      Df F value    Pr(>F)
group  2  13.507 9.771e-06 ***
      75
---
Signif. codes:  0 ‘***’ 0.001 ‘**’ 0.01 ‘*’ 0.05 ‘.’ 0.1 ‘ ’ 1

        Shapiro-Wilk normality test

data:  residuals(aov_fr)
W = 0.89041, p-value = 6.225e-06

[1] 24.86372
```

Figure B-31 Assumptions ANOVA